Chapter 3
Design

Contents

3.1 Thermal Design 51
3.1.1 Single-Core HVDC Cables 52
3.1.2 a.c. Cables 59
3.1.3 Other Factors for the Thermal Design 64
3.1.4 The 2 K Criterion 73
3.1.5 Economic Aspects of the Thermal Design 75
3.2 Design of Mechanical Properties 78
3.2.1 Tensional Forces During Laying 79
3.2.2 The Cigré Test Recommendation 81
3.2.3 Distribution of Mechanical Stress Between Conductor and Armoring 83
3.2.4 Other Forces and Impacts 85
3.2.5 Vortex Induced Vibrations 88
3.3 Electric Design 90
3.3.1 The Concept of Electric Strength 90
3.3.2 The Weibull Distribution 91
3.3.3 Dielectric Design of a.c. Cables 94
3.3.4 Dielectric Design of d.c. Cables 97
3.3.5 Dielectric Design of Mass-Impregnated Cables 100
3.3.6 Impulse Stress 101
3.3.7 Availability and Reliability 102
References 103

3.1 Thermal Design

The aim of thermal design of submarine power cables is to devise a conductor size, which transports the required power without exceeding design temperature limits of the cable or the environment. The thermal design of power cables has been described in many textbooks [1–3] and industrial standards [4] and shall not be repeated here in all details. Instead, this book is supposed to convey an understanding for the

T. Worzyk, *Submarine Power Cables*, Power Systems,
DOI 10.1007/978-3-642-01270-9_3, © Springer-Verlag Berlin Heidelberg 2009

principles of thermal design. Items particular to submarine cables are also touched. Project planners and decision makers may learn about some aspects of the thermal design and especially the aspects related to submarine power cables. For detailed calculations of a particular case, the "cookbook recipes" can be found in the textbooks or obtained from submarine power cable manufacturers.

The basis of all thermal design is a thermal model of the cable. During operation, heat is generated in parts of the cable construction (heat sources), which is transported to the outside of the cable and disappears into the ambient (heat sink). On its way from the source to the sink the heat is traveling through various layers in the cable and in the ambient. The thermal model tries to describe the real situation by a system of equations. With a better knowledge on the cable design and the ambient conditions, a more precise model can be generated. The thermal model must be able to describe continuous and transient conditions.

The cable operator wants to use his assets to achieve maximum benefit without jeopardizing the reliability or useful life of the asset. The benefit from a power cable lies in the accumulated transmitted energy and in the maximum power transmitted at any time. This must be achieved without exceeding the maximum operational limits of the cable.

The cable operator expects answers from the thermal model to at least the following questions:

- Which conductor cross section is necessary for the required transmission power under the given ambient conditions?
- Which short-term overload can I transmit, if the cable already has reached at a certain temperature?
- How does the maximum load change during the annual temperature variations?
- Which regular load pattern can be used under given thermal conditions?
- What happens if other cable operators install cables nearby?

Thermal models with various complexity are available for different purposes. Some simple cases, the dimensioning of a single-core HVDC cable and a pair of HVDC cables in a homogeneous seafloor, are described here to illustrate the basic idea. The symbols are corresponding to those used in the well-known industrial standard IEC 60287 [4].

3.1.1 Single-Core HVDC Cables

The ohmic losses in the conductor are the only heat source in an HVDC cable.[1] The loss P_L can be described as

[1] Most HVDC links have a harmonic spectrum of overtones laying on top of the d.c. current. These overtones create some extra losses which however most often are very small, and are neglected here.

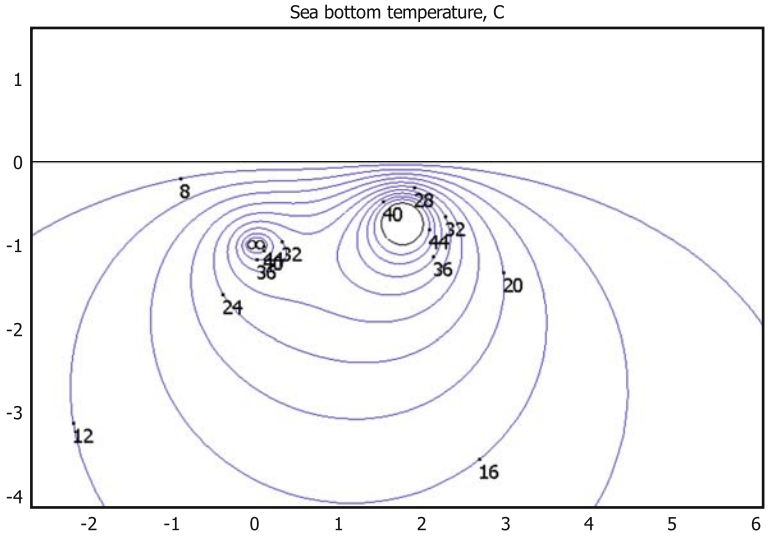

Fig. 3.1 Equithermal lines in an installation of a pair of buried submarine cables (*left*) close to a pipeline (*center*) with 50°C surface temperature. The seafloor temperature at level 0 is assumed to be 4°C

$$P_L = I_C^2 \cdot R' \tag{3.1}$$

where the conductor resistance R' is depending on the temperature:

$$R' = R_{20°C} \cdot (1 + \alpha(\Theta_C - 20°C)) \tag{3.2}$$

Both ohmic losses P_L (W/m) and conductor resistance R' (Ω/m) are given as per-unit-length of the cable. The conductor resistance at 20°C for various conductor sizes is given in Table 3.1. The values apply to conductors made from compressed round wires (IEC 60228 class 2).

Other conductor designs may have, with identical cross section, different resistance values due to other lay length, the presence of water-blocking compound, etc. HVDC cables with Conform-produced profiled conductor wires have often lower resistance values than those in Table 3.1. However, the values above may be used for the thermal design of HVDC cables as they constitute a conservative approximation.

Under steady-state conditions, all the heat generated in the conductor must flow to the outside of the cable. First the heat flows through the cylindrical dielectric insulation. The equation

$$\Delta\Theta = P_L \cdot T_1 \tag{3.3}$$

describes the relation between the temperature drop $\Delta\Theta$ across the insulation wall and the thermal resistance T_1 of the cylindrical insulation wall. For T_1:

Table 3.1 Resistance values for copper and aluminium conductors according to IEC 60228, class 2

	Copper	Aluminium
Specific electric resistivity@20°C, $\Omega mm^2/m$	0.01786	0.02874
Thermal coefficient of the specific electric resistivity @20°C, 1/K	0.00392	0.0042
Conductor resistance according to IEC 60228, Class 2. 20°C	Ω/km	Ω/km
240 mm^2	0.0754	0.125
400 mm^2	0.0470	0.0778
500 mm^2	0.0366	0.0605
630 mm^2	0.0283	0.0469
800 mm^2	0.0221	0.0367
1000 mm^2	0.0176	0.0291
1200 mm^2	0.0151	0.0247
1600 mm^2	0.0113	0.0186
2000 mm^2	0.0090	0.0149

$$T_1 = \rho_T/(2\pi) \cdot \ln(D_o/D_i) \tag{3.4}$$

where D_o is the outer diameter of the insulation screen and D_i the diameter of the conductor. Although the semicon layers of the screens and the insulation have completely different electric properties they have similar thermal properties and therefore they are combined into T_1. The symbol ρ_T denotes the thermal specific resistivity of the insulation material. Table 3.2 lists the specific thermal resistivity for some materials.

In a similar way, the thermal resistance of other cylindrical layers in the cable can be determined. For an arbitrary layer n:

$$\Delta\Theta_n = P_L \cdot T_{(n)} = \rho_T/(2\pi) \cdot \ln(D_o/D_i) \tag{3.5}$$

Table 3.2 Thermal resistivity of cable design materials according to IEC 60287

Insulation	Specific thermal resistivity K·m/W
Paper insulation, oil-filled cables	5.0
Paper insulation, mass impregnated	6.0 (according to IEC 60287)
PPL	5.5
Polyethylene, XLPE or PE thermoplastic	3.5
Polyethylene for extruded HVDC cables	3.5
EPR for cables above 3 kV	6.0
Outer serving	
PE	3.5
PVC	6.0
Polypropylene yarn immersed in water	3.7 (estimated)

with $\Delta\Theta_n$ being the temperature drop over the nth layer. $T_{(n)}$ is the thermal resistance of the nth layer, D_o the outer diameter and D_i the inner diameter of the layer. In our cylindrical single-core cable the total temperature difference between the conductor and the cable surface now is

$$\Delta\Theta = \sum\nolimits_n (P_L \cdot T_{(n)}) = P_L \sum\nolimits_n T_{(n)} = I_C^2 R' \sum\nolimits_n T_{(n)} \tag{3.6}$$

where I_C is the conductor current. The sum runs over all layers in the cable. The thermal model of IEC 60287 defines four thermal layers T_1 to T_4 for the cable and its ambient soil as follows:

T_1: Thermal resistance of the dielectric insulation as defined in Eq. 3.4.
T_2: Thermal resistance between metallic screen/sheath and armoring. This layer also includes bedding layers under the armoring.

$$T_2 = \rho_T/(2\pi) \cdot In(1 + 2\,t_2/D_s). \tag{3.7}$$

where t_2 is the layer thickness and D_s is the outer diameter of the metallic screen/sheath. The extruded plastic sheath over the lead sheath of submarine cables is accounted for in T_2. The bedding is often bituminized fabric tape, sometimes arranged with overlap so that their thermal behavior is difficult to describe. Fortunately the bedding is less than 1 mm in thickness and contributes so little to the total thermal resistance that possible errors in the assumed thermal resistivity are acceptable.

T_3: Thermal resistance of the outer sheath (serving) over the armoring.

$$T_3 = T/(2\pi) \cdot In(1 + 2\,t_3/D'_a). \tag{3.8}$$

where D'_a is the outer diameter of the armoring and t_3 is the layer thickness of the serving/outer sheath. The ρ_T values for some serving materials can be found in Table 3.2.

Metallic screens covering the complete cable can be neglected, as their thermal resistivity is negligible in comparison with that of other cable construction materials. In this context we assume: ρ_T (metal) = 0, $T_{(n)}$ (metal) = 0.

Flat wire armoring with dense laying acts as a consolidated metallic layer and has virtually no thermal resistance compared to other cable layers. An armoring made from round wires, however, is a mixture of metal with low thermal resistivity and air/water/bitumen having a higher thermal resistivity. A detailed differential analysis shows that the composed thermal resistance of a layer of densely packed round wires is at the most 1.5 times the thermal resistance of a solid metal layer of the same thickness. Given the low thermal resistance of metals in the cable construction, we can neglect the thermal resistance of densely packed wire armoring no matter if the interstices between the wires are filled with air or water.

Now, the thermal resistances of all cable layers have been computed. For buried submarine power cables the heat flow continues through the seafloor soil. The accumulated thermal resistance between the buried cable and the sea floor is designated T_4 according to the symbols used in IEC 60827.

3.1.1.1 Single Buried Cable

For a single cable buried in homogeneous sea bottom soil at depth L the thermal resistance T_4 between the cable surface and the seafloor is:

$$T_4 = \rho_T/(2\pi) \cdot In(2\,u) \tag{3.9}$$

where $u = 2L/D_e$, relating the burial depth L to the cable diameter D_e. The burial depth L is defined as the vertical distance between the seafloor and the cable axis (cf. Fig. 3.2). Equation 3.9 is a good approximation for $u > 10$ and applies for most buried cables. For a shallower burial depth of the cable, IEC 60827 suggests more complicated formulae. Typical values for the thermal resistivity ρ_T of the seafloor soil are given in Table 3.6 in Sect. 3.1.3.1.

3.1.1.2 A Pair of Buried Cables

For two identical equally-loaded HVDC cables laid in the same depth, T_4 can be calculated as:

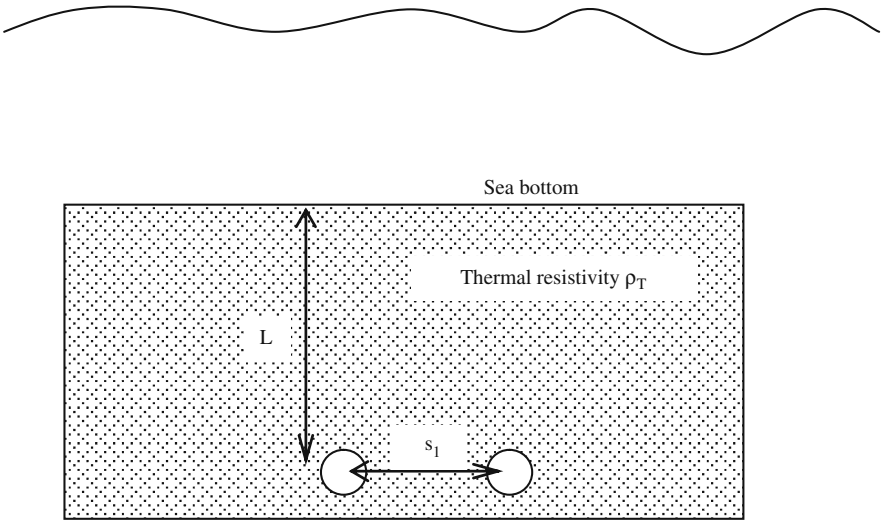

Fig. 3.2 Symbols used for the calculation of T_4

$$T_4 = \frac{\rho_T}{2\pi}\left(\ln\left(u + \sqrt{u^2 - 1}\right) + \frac{1}{2}\ln\left(1 + \left(\frac{2L}{s_1}\right)^2\right)\right) \tag{3.10}$$

For $u > 10$ (which is most often true in submarine installations) the term $(u + \sqrt{(u^2 - 1)})$ can be replaced with $(2u)$.

D_e outer Diameter of the cable/s
L laying depth, as measured from the sea floor surface to the cable axis
s_1 axis distance of the cable pair
ρ_T specific thermal resistivity of the soil material.

The important T_4 value for a pair of identical equally loaded cables can also be found from Fig. 3.3. The figure shows the ratio of T_4 normalized for ρ_T as a function of L/D_e, i.e. the relation between burial depth and the cable diameter. The parameter is the ratio between the burial depth and the cable spacing s_1. Knowing the laying parameters and the cable diameter, the value T_4/ρ_T can be found from the graph. Finally T_4 is obtained by multiplying with ρ_T. Most submarine HVDC cable links can be assessed with Eq. 3.10 as both cables of a HVDC pair are equally loaded and buried at the same depth.[2] Local moderate differences in the burial depth have only little influence on T_4.

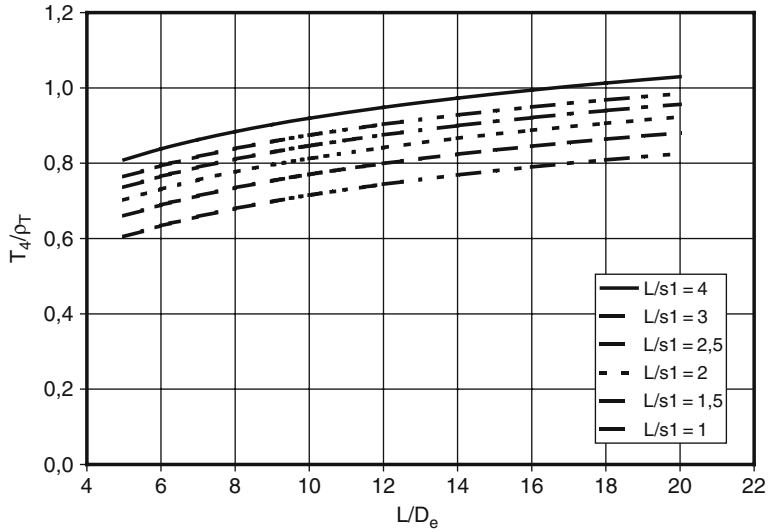

Fig. 3.3 Thermal resistance T_4 of the soil (related to ρ_T) vs. the laying geometry. Denotations are explained in the text

[2]Monopolar HVDC systems with one pole cable and one metallic return cable should be calculated with different equations, as the cables are not identical.

Now we have calculated the thermal resistances T_1 to T_4 and can continue to calculate the ampacity[3] of the HVDC cable as follows:

$$I = \left[\frac{\Delta\Theta}{R'\,(T_1 + T_2 + T_3 + T_4)}\right]^{0.5} \tag{3.11}$$

Here $\Delta\Theta$ is the maximum allowable temperature difference between the conductor temperature Θ_c and the undisturbed ambient soil temperature Θ_{amb}:

$$\Delta\Theta = \Theta_c - \Theta_{\text{amb}}$$

As an example the ampacity of a pair of extruded HVDC cables (Cable type 4) is determined (Table 3.3 and Table 3.4):

The thermal design of most submarine HVDC cables and cable pairs can be performed according to the simple model of Eqs. 3.9 and 3.10. A more detailed calculation is required when both conductors of a HVDC link are combined into one cable, such as in the Kontek, NorNed and Moyle Interconnector.

Table 3.3 Thermal properties of a pair of extruded HVDC cables

Cable design data	
Conductor 1200 mm^2 Cu	$D =$ 39.9 mm
Conductor resistance at 70°C	R(70°C) = 0.0182 Ω/km
Maximum allowed conductor temperature	70°C
Insulation system (1.2 mm semicon, 12 mm insulation, 1.2 mm semicon)	$T_1 = 0.328$ K·m/W
Lead sheath, thickness 2.5 mm	
Plastic sheath, thickness 2.5 mm	$T_2 = 0.036$ K·m/W
Armoring round wires, 5 mm wire dia	
Outer serving yarn thickness 4.0 mm	$T_3 = 0.087$ K·m/W

Conductor tapes, bedding tapes etc are not mentioned but included in the calculations.

Table 3.4 Thermal rating of a pair of extruded HVDC cables

Cable installation data	
Laying depth under the sea floor	1.5 m
Spacing between the cables	5 m
Thermal resistivity of the sea floor	0.8 K·m/W
T_4	0.5423 K·m/W
Ambient temperature in the sea floor	8°C
Current rating	1854 A per cable

[3]The word ampacity denotes the current carrying capability of a cable and has been coined by W. A. DelMar of Phelps Dodge Wire&Cables in 1951 [2].

Mainly two strategies are used to increase the ampacity of the cable system to meet the project requirements: changing the laying parameters (depth and spacing), and changing of the conductor resistance. The use of a larger conductor in order to reduce the conductor losses will cause minor changes in the T_1 to T_4 values. Therefore, the calculation of the optimum cable system is an iterative process.

3.1.2 a.c. Cables

The calculation of a.c. ampacities is much more complex compared to d.c. cables. Additional losses are created in the conductor and the armoring as a result of the alternating current.

3.1.2.1 Conductor Losses

The magnetic alternating field around the conductor current causes the skin effect, by which the current density is low in the centre of the conductor, and high in the outer regions of the conductor. The useful conductor area is reduced, and the effective conductor resistance is increased. The skin effect is more pronounced with increasing conductor areas. Furthermore, the skin effect is depending on the resistivity of the conductor material, the conductor design, and the power frequency. These influences are summarized into the skin effect factor y_s. Since the skin effect adds to conductor losses, the cable ampacity is decreased. Skillful but expensive conductor design can reduce the skin effect considerably especially for large cross section conductors.

Another magnetic effect, the proximity effect, is caused by the proximity of the conductors in a three-phase system. Under the influence of a neighbor conductor, the current strives to concentrate in current paths as far away as possible from the disturbing neighbor. The current density in the conductor becomes inhomogeneous, rendering the conductor portions nearest to the neighbor less useful for current transport. This effect is mostly pronounced for closely spaced large ampacity conductors such as three-phase a.c. cables. The resulting apparent resistance is expressed:

$$R = R'(1 + y_s + y_p) \tag{3.12}$$

where

R is the a.c. resistance of the conductor at maximum operating temperature
R' is the d.c. resistance of the conductor at maximum operating temperature
y_s is the skin effect factor
y_p is the proximity effect factor.

The a.c. resistance R (Ω/m) must be used for the calculation of the conductor losses. The factors y_s and y_p depend on the conductor material and design (stranding, lay-length, segmental or not), impregnated or not, and the power frequency.

Elaborate formulae to calculate y_s and y_p for various cable configurations are given in [2, 3], and shall not be repeated here. For the practical purpose of project planning, it is often enough to know that $(1 + y_s + y_p)$ for small cross section (500 mm^2) most often is below 1.1, i.e. skin and proximity effect increase the effective a.c. resistance of the conductor by less than 10%. Given the uncertainty of the thermal resistivity of the soil, it may be considered to neglect the skin and proximity contribution with small conductors. For very large conductor sizes ($\geq$2000 mm^2), however, skin and proximity effect may enlarge the a.c. resistance with more than 30%.

3.1.2.2 Dielectric Losses

The cable insulation is a dielectric material and can be modeled as combination of a capacitance and a resistance in parallel between the conductor and the grounded screen. Applying a voltage to the conductor results in a capacitive and a resistive current. The resistive current is in phase with the voltage while the capacitive current is shifted with 90°. The resistive current is a loss current generating heat in the insulation. The ratio between resistive and capacitive current is called the loss angle tan δ:

$$\tan\delta = \frac{|I_r|}{|I_c|} = \frac{1}{R_i C\omega} \tag{3.13}$$

where R_i is the resistance of a 1-m-piece of cable insulation (Ω**.**m) and C is the capacitance per meter (F/m). $\omega = 2\pi f$ is the angular frequency of the a.c. voltage. The cable capacitance C can be calculated as:

$$C = \frac{\varepsilon_0 \varepsilon_r}{18 \ln\left(\frac{D_i}{d_c}\right)} \tag{3.14}$$

where D_i is the diameter of the insulation, d_c the diameter of the conductor screen, and ε_r is the relative dielectric constant of the insulation material (Table 3.5).

Now, the dielectric losses in the insulation can be calculated as:

$$W_d = \omega C U_0^2 \tan\delta \tag{3.15}$$

Table 3.5 Dielectric properties of high-voltage cable insulation materials. tan δ is depending on the temperature. A more comprehensive list is in Chap. 12.

IEC 60287	Dielectric loss factor tan δ	Dielectric constant ε_r
XLPE > 18/30 kV	0.001	2.5
EPR	0.005–0.020	3
Oil/paper > 87 kV	0.0033	3.6
Mass-impregnated	0.01	4

The dielectric losses grow with the square of the cable voltage and are relevant only at higher voltage levels. According to IEC 60287, they can be neglected for XLPE cables under 127 kV. For oil-filled submarine power cables being used predominantly for high and extra high voltages, the dielectric losses must not be neglected because of the higher ε and tan δ values. The dielectric losses are not depending on the arrangement of the conductors in single-core or three-core cables, nor on the design of the conductor.

3.1.2.3 Screen Losses

The alternating magnetic field around the conductor generates circulating and eddy currents in the metallic screen and armoring. These currents contribute to heat generation and reduce the cable ampacity. Four different types of induced current losses are considered according to the terminology of IEC 60287:

λ'_1 denotes the losses due to circulating currents in the screen/sheath.[4] Circulating screen/sheath currents occur when the screen/sheath is grounded on both sides of the cable. The losses are depending on the screen/sheath resistance, the screen/sheath inductance, and the arrangement of the phases in relation to each other. Circulating screen/sheath currents can achieve high amplitudes (up to the value of the conductor current) and add a heat source in the cable. The ampacity is reduced considerably. Especially single-core a.c. submarine cables suffer from screen/sheath losses. Loss-reducing measures such as cross-bonding or single-side bonding which are common in onshore cable installations can hardly be arranged for submarine cables.

λ''_1 denotes the losses due to eddy currents in the screen/sheath. The alternatingconductor current generates an emf in the metallic screen or sheath. The emf drives eddy currents locally inside the metallic screen/sheath. The amplitude of the eddy currents is strongly dependant on the thickness of the screen/sheath. The specific resistivity of the materials involved and geometric factors play an important roll. In many cases λ''_1 can be neglected in comparison to the λ'_1 losses. However, λ''_1 should be taken into account for a.c. cables with large segmental conductors, and cables where the λ'_1 losses have largely been reduced by cross-bonding or single-side bonding.

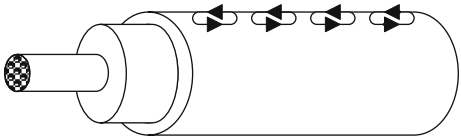

λ'_2 denotes the losses due to circulating currents in the armoring and metallic protection pipes, if applicable.[5] λ'_2 is strongly depending on the total resistance of the armoring layer. Not only the specific resistivity of the armoring material but

[4] "Screen/sheath" includes metallic wire screens (most often Cu wires) and extruded or welded metallic sheathes, but not the armoring.

[5] Sometimes parts of the cable are protected with cast iron half-pipes or similar after installation. This should be taken into account for the cable design.

also the lay-length and contact points between individual wires influence the eddy current losses. Steel wire armorings are particularly affected by eddy current losses as the magnetic material attracts and concentrates the magnetic induction.

An a.c. cable with a low-resistance metallic screen/sheath has a rather high induced screen/sheath current opposite in direction to the conductor current. The magnetic fields from the conductor and the opposite screen current partly cancel each other. For this reason the magnetic effects on the armoring and external pipes are strongly reduced. Single-core a.c. submarine cables sometimes have a large copper screen able to carry the full screen current. As the screen current is opposite to the conductor current, the resulting magnetic field outside the screen is very low allowing for the use of a magnetic steel armoring without excessive armoring losses.

In three-phase a.c. cables the magnetic fields from the individual phases cancel each other to a large extend, which leads to low magnetic losses in the common armoring. Still, the armoring losses cannot be neglected.

λ''_2 denotes the losses due to eddy currents in the armoring and metallic protection pipes, if applicable.

All loss factors λ'_1, λ''_1, λ'_2 and λ''_2 are expressed as a factor relating the losses to the conductor losses. The calculation of the factors is explained for many different cable configurations in [2]. A concise tabular summary is found in [3], all based on the industrial standard IEC 60287, which is commonly accepted as the basis for the thermal design. However, the IEC formulae and factors are sometimes based on empirical values and can be subject to reviews.

For the common type of submarine a.c. power cables having three cores with individual lead sheath and common armoring, the loss factors λ'_1 and λ''_1 are as follows:

$$\lambda'_1 = \frac{R'_S}{R'} \cdot \frac{1.7}{1 + \left(\frac{R'_S}{X'}\right)^2} \tag{3.16}$$

where X' is the reactance of the sheath:

$$X' = 2\omega \cdot 10^{-7} \cdot \ln\left(\frac{2s}{d}\right), \Omega/m \tag{3.17}$$

R'_S is the resistance per meter of the lead sheath, and R' is the resistance per meter of the conductor, s is the axial distance of the conductors and d the average sheath diameter. Unless we deal with large segment conductors (which rarely are used in three-core cables), we can assume

$$\lambda''_1 = 0. \tag{3.18}$$

For the same cable type (≤ 400 mm^2) with common steel wire armoring the losses in the armoring can be summarized as:

$$\lambda'_2 + \lambda''_2 = \lambda_2 = 1.23 \cdot \frac{R'_B}{R'} \cdot \left(\frac{2c}{d_B}\right)^2 \cdot \frac{1}{1 + \left(\frac{3.48 R'_B}{\omega \mu_0}\right)^2} \cdot \left(1 - \frac{R'_S}{R'} \cdot \frac{1}{1 + \left(\frac{R'_S}{X'}\right)^2}\right) \tag{3.19}$$

where:

- c distance between cable axis and conductor axis
- d_B average diameter of the armoring layer
- R_B resistance per meter of the armoring
- R'_S resistance per meter of the lead sheath
- R' resistance per meter of the conductor
- s axial distance of the conductors
- d average sheath diameter.

3.1.2.4 a.c. Cable Ampacity

Three-core a.c. cables have no coaxial geometry, which makes the calculation of the thermal resistivity between conductor and cable surface more complex. While the cable cores (conductor, insulation system, and screen/sheath) are coaxial and can be treated as in single core cables, thermal resistance between the cable core and the common armoring cannot be treated correctly with IEC 60287 methods. The materials in the interstices between the cable cores play an important roll for the heat transport to the ambient. Assemblies of circular polymeric filler ropes, extruded plastic profiles with hollow cores, or even lead profiles are put into the interstices, having much different thermal properties. Extruded plastic profiles with hollow cores are air-filled during manufacturing, but they might fill with water after installation. In these cases, the heat flow and temperature field inside and outside the cable can easily be calculated with commercial FEM software. The mesh generating routines in most FEM software is adaptive with sufficiently high dynamic so that both the temperatures in the small cable details and in the wide cable surrounding can be calculated.

Now the elements necessary to calculate the ampacity of a.c. cables have been collected. The ampacity is expressed as:

$$i = \left[\frac{\Delta\Theta - W_d \left[0.5\, T_1 + n \left(T_2 + T_3 + T_4\right)\right]}{RT_1 + nR\left(1 + \lambda_1\right) + nR\left(1 + \lambda_1 + \lambda_2\right)\left(T_3 + T_4\right)}\right]^{0.5} \tag{3.20}$$

where n is the number of conductors in the cables (one or three). The a.c. resistance R is calculated according to Eq. 3.12. In three-core cables the proximity effect is more accentuated and the a.c. resistance is affected accordingly. The thermal resistances T_1 and T_3 can be calculated according to Eqs. 3.4 and 3.8. The calculation of T_2 for single-core cables can be done according to Eq. 3.7, while the same value for three-core cables is depending on the design of the metallic sheath.

Again, conductor losses and the thermal ambient of the cable are the most dominant factors in the thermal design. Additionally, for a.c. cables the control of losses in screen/sheath and armoring is important to achieve a high ampacity, especially at higher transmission power.

3.1.3 Other Factors for the Thermal Design

3.1.3.1 Transient Conditions

The calculation models shown so far are used to calculate ampacities for steady-state conditions reflecting the case of continuous constant load over long time. In real life, cables are rarely operated at constant load over a longer time. Knowing that, the thermal design of a given submarine cable project can be reconsidered. For this, it is important to know how fast the cable temperature increases after the load is switched on, and after which time the cable reaches a steady-state condition under the impact of a constant load. Taking into consideration the load variations over time, one can perform a transient cable rating.

The mathematical challenge is to express the temperature response of the different cable layers and its surrounding on a step function representing the power switch-on. In the 1950s, when computers were not commonly available, many researchers suggested analytical solutions before Neher/McGrath published their famous papers in 1964 [5, 6], which subsequently influenced the IEC standard 60287.

The thermal models of power cables represent the various layers of the cable by thermal resistances and thermal capacitances. The heat dissipated in the conductor travels through the thermal resistance of the insulation and the outer layers towards the ambient soil.[6] The analogous network shown in Fig. 3.4 is called a Cauer-type RC ladder network. Cauer networks are often used to calculate heat flow phenomena in semiconductor devices.

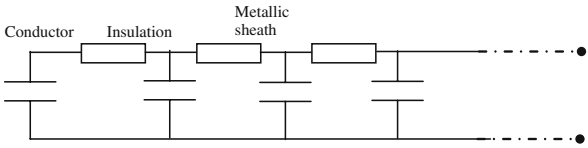

Fig. 3.4 Cauer-type ladder network representing a cable construction

The ladder network consists of the thermal resistances R of the various cable layers and the ambient soil, and capacitances C, which represent the thermal capacities of the different cable layers and the ambient soil. The thermal capacitance of a given volume V of a material with the specific heat c_p is:

[6] In the electric analogy the conductor loss corresponds to a current source, the heat flow from the conductor outwards corresponds to an electric current, the thermal resistance of each layer corresponds to an electric resistance, and the thermal capacitance of each layer corresponds to an electric capacitance.

$$C = c_p \cdot V \cdot \rho_G$$

where ρ_G is the density of the material.

Let us consider a simplified fictitious cable, only consisting of a 1200 mm^2 copper conductor and a 12 mm polymeric insulation, directly submersed into water. The outer surface of the cable is kept at 10°C by ambient water. At $t = 0$ the load is switched on, generating a constant conductor loss of 30 W/m irrespectively the conductor temperature. The conductor losses heat up the thermal capacitance representing the conductor (solid line in Fig. 3.5), and the conductor temperature follows a logarithmic curve until a steady-state condition at about 18°C. The increasing temperature difference between the conductor and the ambient causes an ever-increasing heat flux (dotted line in Fig. 3.5) through the thermal resistance representing the insulation. The increasing heat loss through the insulation reduces the thermal power available for heating up the conductor, and the steepness of the temperature rise curve declines. A classical thermal time constant $\tau = R.C$ can be defined for this simple system. The time constant of this system is 1220 s as indicated by an arrow. After 1220 s, the temperature rise has reached 63% of its final value.

In a real cable installation, there are more thermal resistances and thermal capacitances coupled into a ladder network. Some layers, such as a lead sheath, can simply be represented by a thermal capacitance, while their thermal resistance can be neglected due to the high thermal conductivity of the metal. Insulation layers of a few millimetres thickness can be modelled by a single thermal resistance and a single thermal capacitance. Thicker insulation layers must be subdivided in a number of "onion shells" each of them with its own resistance and capacitance. Many computer-based models of the thermal ladder comprise 20 layers or more. A further complication is that in many high-voltage a.c. cables heat sources exist outside

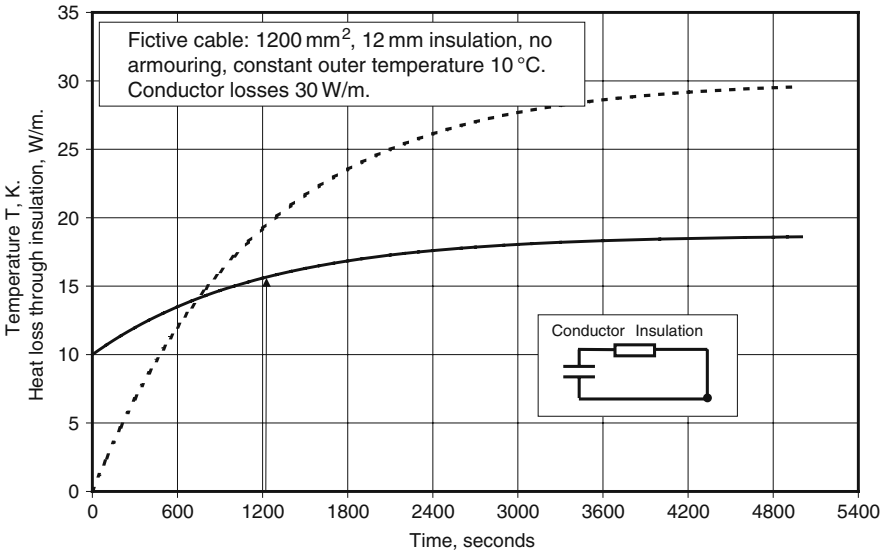

Fig. 3.5 Temperature evolution (*solid line*) and heat flow through the insulation (*dotted line*) in a fictive simplified single-core cable

the conductor, such as dielectric losses and sheath/screen/armoring losses. It is not possible to define a classical thermal time constant for these complicated systems, as the step response is not longer a simple logarithmic rise such as in Fig. 3.5.

The ambitious reader may find exhaustive reading on the subject in [2, 7]. However, a few further considerations are important for the understanding of the cable behaviour and rating.

3.1.3.2 Temporary Overload

Today, submarine power cables are usually buried 1–3 m down in the seafloor. The seafloor temperature will rise slowly, heated by the cable losses. The constant ambient temperature assumption in the simple model of Fig. 3.5 is not valid anymore. Since the seafloor has a large thermal capacitance and a large thermal resistance due to its sheer size, it can take weeks or months to warm up the seafloor around the cable to steady-state conditions. Although a time constant in a classical sense can no longer be defined, it can be useful to use two "quasi"-time constants to characterize the complex system of cable and surrounding soil. The thermal time constant τ_c of the cable describes the response of the conductor temperature to a step-formed load change, while the soil time constant τ_s describes the response of the soil temperature to a long-term load in the cable. Even for the most massive submarine cables, τ_c is in the order of 0.5–2 h. In contrary, τ_s is in the order of weeks or months. This dual time response behavior has some important consequences.

The evolution of temperature in and around a submarine cable is illustrated in Fig. 3.6. It starts with the "all-cold" situation (curve No. 1) where the cable and

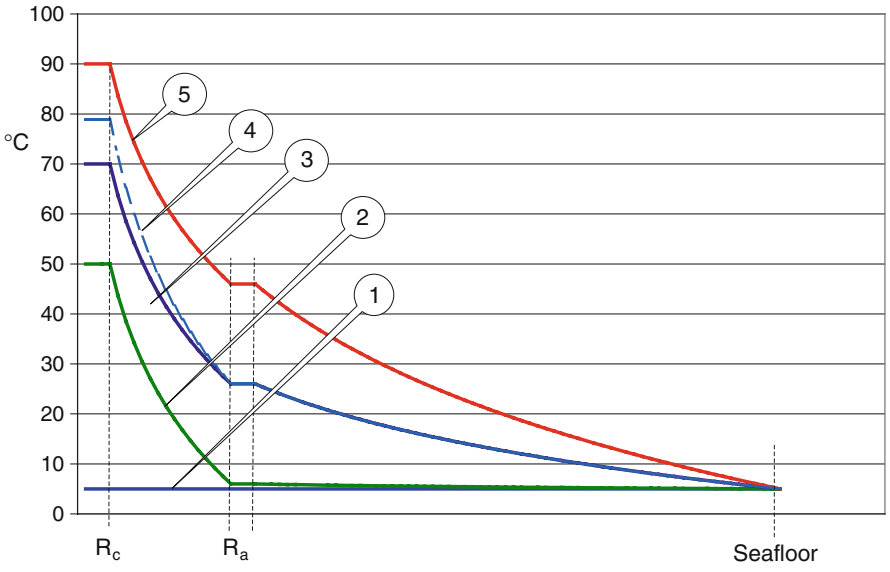

Fig. 3.6 Temperature profile in a single-core cable and surrounding soil

the seafloor have the same undisturbed temperature, being 5°C in our example. The x-axis of Fig. 3.6 indicates the distance from the conductor, where R_c denotes the conductor radius, R_a the radius of the armoring, and the label "Seafloor" indicates the position of the surface of the sea bottom.

Now we put full rated load on the cable from "all-cold" condition, and the cable will reach a first steady-state after 3–4 times τ_c, i.e. a few hours. This situation is indicated in curve 2 of Fig. 3.6. It is also visible that the temperature curve inside the conductor is flat because the metal equalizes all internal temperature gradients. The conductor temperature reaches 50°C in this example. During this time, the ambient soil (between R_a and "Seafloor") changes its temperature only very little.

Under continued rated load, the soil temperature rises slowly as a result of the dissipated heat from the cable. At the same pace as the soil temperature next to the cable surface rises, the cable conductor follows suit. An intermediate situation is depicted as curve no. 3 in Fig. 3.6. As the soil and thus the cable armoring (at R_a) slowly increase in temperature, the conductor temperature keeps pace by always holding 45 K over the cable armoring. The temperature difference between armoring (at R_a) and the conductor stays constant, as this is only dictated by the conductor heat losses, which are assumed to be constant.[7] Finally, still under constant rated load, the system arrives at a steady-state indicated by curve no. 5 in Fig. 3.6. In the steady-state value the conductor temperature has arrived at 90°C and the cable surface (armoring) temperature is at 46°C.[8]

Let us go back to the situation of curve no. 3 in Fig. 3.6. The cable had been operated at full nominal load for days or even some weeks. Temperatures have not reached their final steady-state value yet. It is obvious from the graph that the conductor temperature is below the maximum temperature that it is designed for (90°C), and that it would reach only some weeks later. Meanwhile, we could use the thermal reserve to run temporary overload on the cable. Higher current means larger ohmic losses in the conductor, a larger heat flow through the insulation, and a larger temperature drop over the insulation. This renders a steeper temperature curve between R_c and R_a as indicated in curve no. 4 in Fig. 3.6. The overload can only be run 0.5–2 h until the conductor temperature reaches the design limit and must be reduced subsequently. Different restrictions may apply for HVDC cables as they usually have a maximum allowed temperature difference across the insulation.

A different starting case for a possible temporary overload occurs when the cable has been run with reduced load for a long time. In the following section, the possible overload for short periods is estimated with some easy equations. Recall the calculation of the maximum continuous current I_{cont} according to Eq. 3.21:

$$I_{\text{cont}} = \left[\frac{\Delta\Theta}{R' \left(T_1 + T_2 + T_3 + T_4\right)} \right]^{0.5} \tag{3.21}$$

[7] For the sake of simplicity, we neglect here that the conductor resistance and hence the losses increase with the conductor temperature.

[8] This value is only valid for this example. Cable surface temperatures are depending strongly on the specific case.

The steady-state conductor temperature Θ_c is according to Eq. 3.21:

$$\Theta_c = \Theta_{\text{amb}} + I_{\text{cont}}^2 \cdot R' \cdot \sum \cdot T_i \tag{3.22}$$

When the same cable had been running at 75% load ($I_{75\%} = 0.75\ I_{\text{cont}}$) the steady-state temperature, accordingly, would have been:

$$\Theta_{75\%} = \Theta_{\text{amb}} + I_{75\%}^2 \cdot R' \cdot \sum \cdot T_i = \Theta_{\text{amb}} + 0.75^2 I_{\text{cont}}^2 \cdot R' \cdot \sum \cdot T_i \tag{3.23}$$

The steady-state temperature $\Theta_{75\%}$ at 75% load is lower than the full load temperature and the difference is $\Theta_c - \Theta_{75\%}$. Now, we switch on the overload current I_{overload}. For a short-term overload (say 10 min), we may assume a quasi-adiabatic situation where the excess heat is only used to heat the conductor but the heat flow through the insulation is maintained at the level of the 75% constant load prior to overload. For an overload time of 10 min = 600 s, we can establish:

$$(I_{overload}^2 \cdot R' - I_{75\%}^2 \cdot R') \cdot 600\,s = c_p \cdot m_{Cu} \cdot (\Theta_c - \Theta_{75\%}) \tag{3.24}$$

The left side of the equation is the difference between the loss power $I^2{}_{\text{overload}}\%R'$ and the power outflow $I^2{}_{75\%}{}'R'$ through the insulation, multiplied with the duration of the overload current. This is the excess energy that is consumed by the heating of the conductor. c_p=393 J/(kg K) is the specific heat of copper, and m_{Cu} is the mass of one meter of the copper conductor. For a cable with a 1200 mm^2 Cu conductor we find that I_{overload} (10 min) = 3513 A. This is indeed an amazing figure of overload after a long continuous load of 75% of nominal load.

The temporary overload calculation according to Eq. 3.22 may be applied to a.c. cables where the electric stress in the insulation is not depending on temperature gradients. The same algorithm can be applied to overload durations shorter than 600 s, to different pre-overload load factors (instead of 0.75), or to aluminum conductors by accordingly adjusting the parameters.

For d.c. cables an additional restriction applies. The temperature difference over the insulation must not exceed a specified value in order to stay below a specified electric stress in the insulation. Equation 3.24a would thus transform for d.c. use:

$$(I_{\text{overload}}^2 \cdot R' - I_{75\%}^2 \cdot R') \cdot 600\,s = c_p \cdot m_{Cu} \cdot (\Delta_{\max} - \Delta\Theta_{75\%}) \tag{3.24a}$$

with $\Delta_{\max}$ the maximum specified insulation temperature drop, and $\Delta\Theta_{75\%}$ the insulation temperature drop at 75% load.

For longer overload periods, the time-dependent heat outflow through the different layers must be taken into account.

From the situation depicted in curve no. 3 of Fig. 3.6, another overload scenario is also possible. If only a little overload is run, e.g. 15% over full load, the temperature difference over the insulation would soon (within 3–4 times τ_c) assume a new value somewhat larger than the difference at full load. But the conductor temperature would not reach the limit in the first place. Now, we have a non-adiabatic

process where the excess heat from 15% overload has time enough to flow outwards through the different layers. It slowly heats up the surrounding soil. As the soil slowly increases in temperature, the conductor temperature keeps pace. When it arrives at the limit (=90°C in Fig. 3.6), the load must be reduced to 100% load to avoid overheating.

Power cables with direct contact to the free sea water (unprotected, laid directly onto the seafloor or in spans) cannot use the benefits of the thermal capacitance of the surrounding soil. The surface temperature of these cables follows the seawater temperature, which is changing only very slowly through the year. The exposed cables will reach steady-state conditions after only a few hours. The overload capability of exposed un-buried cables is much lower compared to buried submarine power cables.

3.1.3.3 Cyclic or Variable Loads

Most submarine power cables are operated with varying load, which is often below the rated power transmission. These cables are under-utilized during certain periods, and the operator might be interested in extra transmission power during peak demand.

Some cables, predominantly those feeding populated islands, may have a daily cyclic load pattern. IEC 60853 has developed algorithms to calculate possible overload due to cyclic cable utilization. The methods are based on the calculation of an average loss factor through the day, such as indicated in Eq. 3.25. The fact that the cables have a daily load pattern can be exploited in two different ways:

1. A higher short-term ampacity can be offered during and past the periods of lower load.
2. A smaller conductor size can be chosen if the load pattern is guaranteed.

Another actual case of variable loads is the submarine connection of OWPs. Most of the time the load in wind-farm cables (both in-field connectors and export cables) is below rated OWP output power. The duration of peak loads is counted in few days at each time. The short-time peak loads are efficiently equalized by the large time constant of the sea soil. A statistical analysis of the expected wind conditions can result in lower cable load requirements and appreciable investment cost reductions [8]. For the unlikely case of long-lasting full-power wind generation, on-line cable temperature monitoring can advise the operator to shut down some turbines if necessary.

However, it must be remembered that unburied submarine cables have no thermal reserve from the ambient soil; they offer very little overload capabilities.

3.1.3.4 Thermal Resistivity of the Seafloor

For good reasons, one of the prime objectives of any cable design is to avoid hotspots as they can jeopardize the availability of the link. It is therefore extremely

important to have a detailed knowledge of the thermal surrounding of the cable, i.e. the thermal resistivity of the seafloor and the ambient temperature. Actually, the precise knowledge of these parameters along the cable route can save investment money and/or increase availability and lifetime.

The thermal resistivity of soil is a function of the soil base material, the dry density, the distribution of grain size, the compaction, the humidity and the content of organic materials. The influence of humidity, one of the most important factors for land based soils, can be disregarded in subsea soils because the soil is completely soaked. This is also valid for seafloors of tidal flats which fall dry during low water tide. The German Maritime Authority (BSH, Bundesamt für Seeschiffahrt und Hydrographie) assumes a thermal resistivity of 0.7 K·m/W or less for soil saturated with water [9]. Values up to 1.03 K·m/W have been found in in-situ measurements in the North Sea [10]. Other measurements show values as low as 0.5 K·m/W [11]. Further values are shown in Table 3.6.

The large distribution of these values and those found in Table 3.6 implies that it is one of the most important objectives of the marine survey to measure the thermal resistivity of the soil along the cable route. The measurement of thermal resistivity values for soil is rather delicate. Soil samples taken from the intended installation site can represent the soil base material, grain size distribution, and, in case of submarine soil samples, the humidity content. However, the in-situ degree of compaction is difficult to reproduce in the laboratory. The degree of compaction might be different in virgin soil and in soil after cable laying and burial.

The soil conditions in the vicinity of the submarine cable can be inhomogeneous due to geomorphologic or anthropogenous factors. As an example, the cable is perhaps installed in layered soils or in trenches, which are being filled with non-local material. Also the protection of submarine cables with rock-dumping or concrete slabs creates inhomogeneous thermal ambient conditions. Commercial FEM software can solve the task to find out the effective thermal insulation of an inhomogeneous cable cover that is composed of different soils/rocks/items.

It is important to create a complete picture of the soil conditions along the entire cable route before doing the cable design. The locations of the limited number of soil samples should be chosen so that the thermal properties of the cable route can be mapped in sufficient accuracy.

Table 3.6 Thermal properties of some submarine soils

	Heat capacity per volume $\rho \cdot c_p$, MJ/(m^3·K)	Thermal Resistivity ρ_T	
References	[12]	[12]	[13]
Gravel	2.4	0.55	0.33–0.5
Sand	2.2–2.9	0.2–0.59	0.4–0.67
Clay/silt	1.6–3.4	1.0–2.5	0.56–1.11

3.1.3.5 Ambient Temperature

The ambient temperature is a critical value in all thermal design calculations, no matter which method is used, or which load cases are considered. The ambient temperature for the cable is defined as the temperature at the *locus* of the cable if the cable would *NOT* be there, i.e. the undisturbed ambient temperature.

For unburied submarine cables, the ambient temperature is simply the temperature of the seafloor water. Even when the surface water temperature may change considerably over the year the water temperature at seafloor level can be quite constant but that is not the case everywhere. At some locations in the North Sea, the seafloor water temperature fluctuates between 8 and 17.5°C during the year. Relevant data for a specific submarine cable project can often be obtained from the national hydrographical institute or commercial survey companies. The highest summer temperature of the seafloor water is different in different years. Statistics list 10-years-high, or 100 years-high values. It is up to the decision of the cable owner/operator which of these values should be used in the context of the overall asset management.

When the unburied cable is carrying load, its surface temperature is only a few degrees over the ambient water temperature. Flowing water provides a better assimilation of temperatures compared to calm water. However, a thermal cable design should not be based on the assumption of the beneficial effects of flowing water.

For the thermal design of buried submarine cables, the ambient temperature at the burial depth must be taken into account. The annual variation of the water temperature at the sea floor penetrates down into the sea bottom until it reaches the intended cable position and beyond. In deeper depths under the seafloor, the amplitude of the seasonal variation becomes smaller and the peak value occurs later in the year. The schematic course of the temperature is shown in Fig. 3.7. Assuming an annual average temperature T_a on the seafloor and a sinusoidal course of the seafloor temperature, the annual variation of the temperature in the depth z can be described as [14]:

$$T(z,t) = T_a + A_0 e^{-z/d} \sin\left(\frac{2\pi(t - t_0)}{365} - \frac{z}{d} - \frac{\pi}{2}\right) \tag{3.25}$$

T (Z,T) Temperature at time t in the depth z
T_a Average temperature at the seafloor averaged over the year
A_0 Amplitude of the annual variation of the seafloor temperature
d penetration depth of the annual temperature variation
t_0 Constant reference time.

The penetration depth is $d = (2\ D_h/\omega)^{1/2}$ with D_h being the thermal diffusity (cf. table 3.7). $\omega = 2\pi/365$ is the angular frequency of the annual variation, denoted in 1/day.

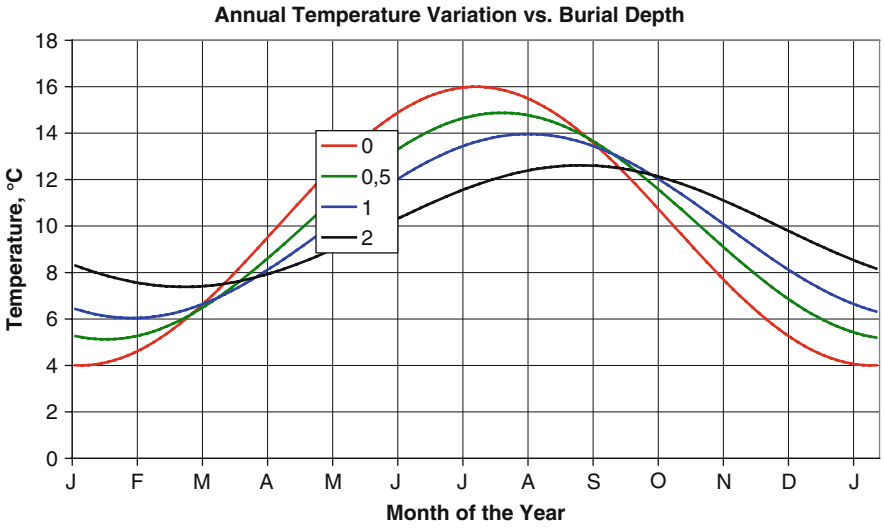

Fig. 3.7 Schematic course of the temperature as a function of time and depth. The depth parameter is given in *metres*. Assumed thermal diffusity $D_h = 0.05$ m^2/day

Table 3.7 Empirical relationship between thermal diffusivity and thermal resistivity for homogenous and moist soils, according to IEC 60853-2 App. D

Thermal resistivity (m×K/W)	Thermal diffusivity (m^2/day)
0.35	0.0864
0.45–0.54	0.0691
0.55–0.64	0.0605
0.65–0.84	0.0518
0.85–1.04	0.0432
1.05–1.24	0.0389

The parameters of Eq. 3.25 can be determined by plotting the annual variation of seafloor temperature. From this, the average temperature at the seafloor T_a, the amplitude of the annual variation A_0, and the reference time t_0 can be determined. For all further calculations at various depths the same t_0 is used.

In the example of Fig. 3.7, the soil temperature at 1 m burial depth reaches a peak of 14°C. The cable that will be buried here can be designed for 14°C ambient temperature instead of 16°C which is the maximum temperature at the seafloor. Note that Fig. 3.7 is just an example showing the principal course of temperatures. For every submarine power cable project the values T_a and A_0 should be identified. If they cannot be retrieved from long-term measurements the estimated values should have sufficient safety margins.

3.1.3.6 Conditions Changing with Time

Seafloor conditions, which have been charted by survey operations, may alter during the cable's lifetime. While water temperature hopefully increases only slowly with the climate change, other parameters may change faster.

Coastal waters exposed to tidal currents are subject to strong and fast changes of the bathymetric structure. Spring tides and storms can cause erratic changes. A cable buried at the –2 m level might be exposed to water, or covered underneath 10 m of sediment. These unpredictable changes have nevertheless to be taken into account for the cable design.

The thermal ambient of submarine cables can also be changed by human activities such as dredging, dumping, etc.

Submarine cables can be subjected to marine growth. The submarine fauna/flora may create extensive layers of organic material over buried cables, which has the effect of thermal insulation and consequential overheating of the cable. Cables on a free span, covered with a thick layer of subsea dwellers, may constitute dangerous hot-spots in the cable route.

3.1.4 The 2 K Criterion

The prospective of a massive installation of offshore wind parks triggered a discussion of the heating of the seafloor. Environmentalists and authorities mainly in Germany advocate a limitation of the expected warming of the seafloor above the submarine power cable (cf. Chap. 10). According to this discussion, the seafloor above the cable must not be warmed up more than 2 K over the undisturbed temperature. The warm-up is calculated for a reference location straight above the cable, at a depth of 0.2 or 0.3 m under the seafloor surface.[9] By means of FEM software the situation can be calculated easily. This chapter provides a simpler method to determine the warm-up for many cases. We use the following terminology.

$\Delta\Theta_{0.2}$ is the temperature rise over the undisturbed sea soil, at a depth of 0.2 m under the seafloor. $\Delta\Theta_{0.3}$ is the corresponding value for a depth of 0.3 m under the seafloor. Both values are valid for steady-state conditions, which are reached only after weeks of continuous constant full load. We consider two representative types of cable installation configurations:

1. A pair of cables laid touching. HVDC cables are sometimes installed in this configuration.
2. A single cable. This represents the case of a three-phase a.c. cable, or one single-core cable in a group of cables laid with distance. In submarine installations, cables are installed either in a bundle (cf. case 1) or with a lateral distance of 5 m or more due to installation restrictions. In the latter case, each cable of the group can be considered as a single cable.

[9] Different authorities and environmental groups use either 0.2 or 0.3 m.

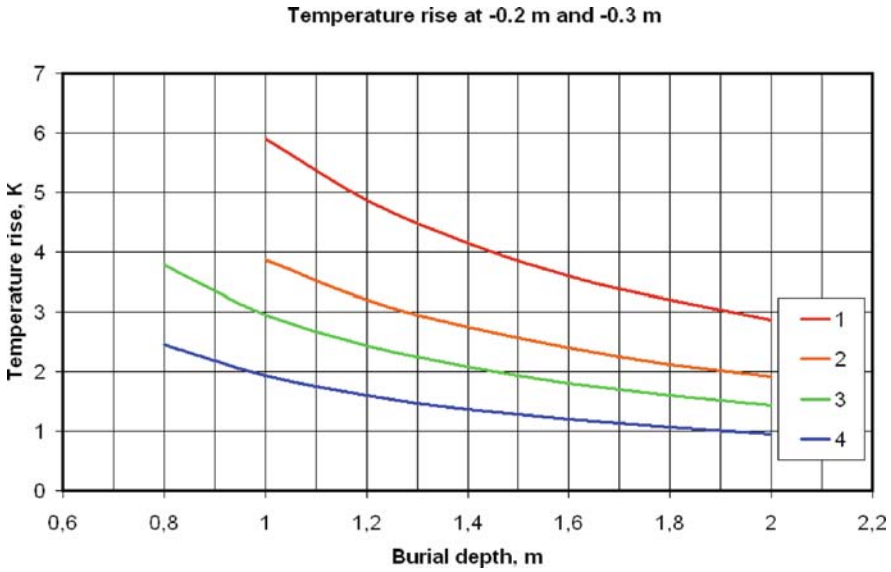

Fig. 3.8 Temperature rise over the undisturbed seafloor. Curve 1: A pair of HVDC cables, touching, cable diameter 100 mm, –0.3 m; Curve 2: A pair of HVDC cables, touching, cable diameter 100 mm, –0.2 m; Curve 3: A single cable, diameter 150 mm, –0.3 m; Curve 4: A single cable, diameter 150 mm, –0.2 m

The curves in Fig. 3.8 are calculated for a cable loss of $P_{\text{loss}} = 30$ W/m in each cable, and a thermal resistivity of $\rho_T = 1.0$ K·m/W. The temperature rise in a specific project can be calculated as follows:

To find out the temperature increase $\Delta\Theta_{0.2\text{ m, project}}$ at the –0.2 m level for any project the following equation shall be used:

$$\Delta\Theta_{0.2\,\text{m,project}} = \Delta\Theta_{0.2\text{m}} \cdot \rho_T \cdot \frac{P_{\text{loss,project}}}{30\,W/m} \tag{3.26}$$

where $P_{\text{loss, project}}$ is the total cable loss in the actual project. $\Delta\Theta_{0.2}$ is taken from Fig. 3.8. The actual thermal soil resistivity goes in as ρ_T.

Accordingly, the temperature increase $\Delta\Theta_{0.3\text{ m, project}}$ at the –0.3 m level can be calculated from the values in Fig. 3.8 and the actual cable losses and thermal resistivity.

The cable diameter has only little influence on the resulting temperature rise. A case with a single cable with 190 mm diameter has been calculated. The results differ from the values of the 150 mm cable only in the second decimal place.

The results presented in Fig. 3.8 are strictly spoken valid for steady-state conditions only. However, they can also be used for cases where the cable load is subject to daily cyclic patterns. The large thermal inertia of the seafloor equalizes the daily variations. Starting from the daily load pattern an average cable loss value can be calculated from the mean square I_{24} of the current during the day:

$$P_{\text{loss,average}} = R \cdot s \cdot \frac{1}{24\ \text{h}} \cdot \int_0^{24} I^2(t)\, dt \tag{3.27}$$

where

I(t) the conductor current as a function of time. The integral adds up one current value for each hour for the day.
R resistance of each phase.
s number of phase conductors in the system.

The average loss during a 24-h period is often considerably smaller than the cable losses at full rated load. This should be taken into account when using Eq. 3.26 for the calculating of the soil warm-up.

3.1.5 Economic Aspects of the Thermal Design

When designing a power cable it is attempting to reduce the conductor size as much as possible in order to reduce the tender price. This design method results in the smallest conductor meeting the ampacity requirements and the smallest initial costs. Indeed, for longer submarine cable links, the slightest reduction of the conductor size can save appreciable amounts of investment. For a 100 km link the cross section reduction with only 10 mm^2 copper can save some 36.000 US$ in copper costs per conductor.[10] However, it became clear decades ago that the costs of losses must not be neglected. A larger conductor cross section reduces the losses and associated costs over many years ahead. A comprehensive cost analysis includes not only the up-front investments (Capex) but also the cost of losses during the cable lifetime. Here, we try to sort out what the loss evaluation factor is, and how it can translate to the conductor size with the lowest lifetime costs for the investor.

The total lifetime costs of a cable system include the investment and the accumulated future costs of losses and maintenance. The future operational costs (Opex) can be projected to the present time with "present value" methods. The question is whether or not the smallest conductor size from the thermal point of view generates the smallest lifetime costs.

The assessment of the present value of future cable losses starts with the calculation of the losses Q_L in one year. The accumulated losses over a year in the cable system are:

$$Q_L = I_0^2 \cdot R \cdot s\mu \cdot 8760\, h \tag{3.28}$$

where

I_0 nominal maximum conductor current
R equivalent resistance of each phase

[10] Assumptions for the calculations in this chapter: Copper price 4000 US$/ton.

s number of phase conductors in the system
μ load loss factor of the cable link

The equivalent resistance includes all load-depending losses such as ohmic conductor losses, the contribution of skin and proximity effects, and the contribution of armoring/screen/sheath losses. Dielectric losses are neglected here. The load loss factor μ is the normalized mean square of the current over time.

$$\mu = \frac{1}{8760\ \text{h}} \cdot \int_0^{8760} \frac{I^2(t)\,dt}{I_0^2} \tag{3.29}$$

I(t) is the average conductor current in each hour of the year. For a cable system running on full power over the year $T\mu = 1$. For a cable link to be built in the future, it is not easy to determine the integral in Eq. 3.29. Meanwhile some rough assumptions can be made:

$$\mu = p \cdot m + (1 - p) \cdot m^2 \tag{3.30}$$

with $p = 0.3$ for transmission lines and $p = 0.2$ for distribution lines [2]. m is the load factor, i.e the normalized average current (not square) over time.

We can reduce the future loss costs to the present value C_L at the time of investment:

$$C_L = \frac{C \cdot Q_L}{i} \cdot \left[1 - \left(\frac{1}{(1+i)^n}\right)\right] \tag{3.31}$$

where

C Cost of 1 kWh of electricity to cover the losses ($/kWh)
i Rate of interest on the capital market
n Cable lifetime (years).

This formula can be used both for a.c. and d.c. cables. It is valid under the (uncertain) assumption that C, L, and i are constant over the n years of lifetime, which is a strong simplification. Calculation procedures including variable load schemes and variable loss unit costs C over the years are given in [2]. With the equations given above the present value C_L of future loss costs can be calculated. This value is often given to the cable manufacturer in the cable system specification in "dollar per kW" units. Each kW of cable losses is penalized with a sum of money reflecting the accumulated C_L costs of the losses over the entire cable lifetime.

Figure 3.9 illustrates the conditions under which it is profitable to increase the copper cross section, depending on the combination of copper price and energy price during the lifetime of the cable. The assumptions are:

- Cable design (1200 mm^2 HVDC) according to Table 3.4
- Ampacity 1854 A rated maximum current

- Lifetime 30 years
- 7% capital costs
- Cable price increases linearly with the LME copper price times a factor 1.5 for manufacturing
- The calculation is made for an upward step from 1200 to 1210 mm^2.

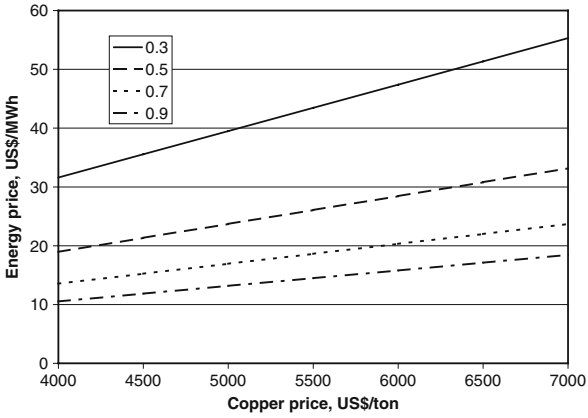

Fig. 3.9 "Break-even" values for the cable described in Table 3.4. At energy prices over the curve it is profitable to increase the copper cross section

The load loss factor μ is the curve parameter. It is profitable to increase the copper cross section if the energy price is higher than the value stated in the diagram. The incremental cable price indicated above is nothing but an assumption for incremental cable price changes and must not be taken as an indication for cable prices based on LME copper values.

By nature, all theories are based on assumptions on the future value of some parameters, which tend to be very volatile:

The technical lifetime of a cable system can be anything between 10 and 40 years.[11] The lifetime is a statistical number. Most manufactures would agree on a 30–40 years expected lifetime for a well-protected submarine cable.

Capital market terms will vary largely during this time, and so will the rate of interest. Since an investor would probably finance the investment with a mix of loans with different terms it is not possible to put a single rate of interests into the formulae. The often used Eq. 3.34 is not very useful in these cases.

Generation costs for losses are often equal to the electricity price on the upstream side of the cable link. This price changes by the hour for trading links. For OWP the loss costs can be assessed from different viewpoints as explained in Chap. 10. In any case, the costs for losses are not constant or even known over the cable lifetime.

Installation criteria. If there are requirements to keep a certain low sediment temperature over the buried submarine cable, it could be advantageous to reduce

[11] Some submarine cable installations have had lifetimes below 10 years or over 40 years, and may be considered as statistical outliers.

Table 3.8 Estimated utilization of submarine power cable links

Type of submarine link	Link utilization
Supply of islands with residential demand	According to island demand, 4380/8760 h
Supply of G&O platforms	90% 7884/8760 h
OWP	25% 2190/8760 h
Power trading between autonomous grids	70% 6130/8760 h

the cable heat losses by extra conductor copper. A larger conductor emits less heat and can be buried shallower for less money to meet the 2 K criteria. At the end, the larger conductor might induce lower costs.

Cable utilization. The utilization of a submarine cable link depends largely on the type of the application (cf. Table 3.8). For a specific cable link the utilization may vary largely from week to week and over the years.

Recycling costs/benefits after the cable lifetime. Regulators today sometimes require that cable systems must be recovered after the end of life. If this is the case, the conductor copper is not a write-down investment. In contrary, increasing metal prices can turn the cable copper into a valuable asset. Extra copper in the conductor would not only reduce costly losses but also would contribute to late income when recovering the cable.

All these imponderables make the standard economic evaluation methods little useful. Some trends are visible:

- For a short expected lifetime the Capex are more important than the Opex. Select the conductor area as small as possible with respect to thermal conditions.
- For a long expected lifetime the Opex may outweigh the Capex. It might be attractive to put in more copper to reduce costly losses.
- High energy prices bring the focus to the loss reduction. Losses must be paid for somewhere, and the value of some extra copper in the cable becomes more attractive with increasing energy prices.
- An OWP owner might consider investing into a larger conductor size. To bring the same amount of power to shore, it is better to invest in a maintenance-free increase of cable cross section compared to another turbine needing annual maintenance.
- If the cable is to be recovered after life, the investment in extra copper is even more attractive due to future metal prices.

3.2 Design of Mechanical Properties

Submarine power cables must be designed to withstand all mechanical stresses during manufacturing, handling, transport, installation, and operation. The stresses imposed to submarine power cables are much different from those imposed to underground cables. An inappropriate mechanical design has the potential to leave the

cable vulnerable to damages with the possible consequence of higher unavailability and large repair costs. As a result of poor mechanical design, some cable systems had to be abandoned or replaced by new ones long before their electrical lifetime was over.

The first challenge is to bring the cable safely into the water. The armoring has to provide sufficient tensional strength. The required tensional strength for a submarine power cable project is primarily a function of the water depth. Dynamic forces during the installation may impose much stronger requirements, and conditions during the operation, such as strong currents or forces in cables hanging in free spans, may add to the tensional strength requirements.

3.2.1 Tensional Forces During Laying

When the cable is being laid from a cable ship there are at least four components that contribute to the tensional forces at the laying wheel:

- Static weight of the cable between the laying ship and the seafloor.
- Residual bottom tension, which translates to an extra tensional force at the laying wheel.
- Extra weight of the catenary line between the laying wheel to the touch-down point (TD) on the seafloor.
- Dynamic forces when the laying wheel is moving up and down.

The static tensional force is $T_s = w \cdot D$, with w being the unit weight of the cable in water and D being the water depth. The small length of cable between the water surface and the exit point on the laying wheel[12] is neglected here.

During laying the cable is not just let down vertically. Instead, the cable must be positioned in a well-defined catenary line from the laying wheel to the TD by application of a certain tension in an on-board cable break device. Under these circumstances the cable hits the sea floor asymptotically.

The shape of the catenary is associated to a certain bottom tension. The length of the catenary line is longer than the water depth resulting in a larger weight of cable hanging in the laying wheel as if the cable would hang down vertically (cf. Fig. 7.28). The top tension T , i.e. the tension in the cable at the laying wheel, is expressed as:

$$T = \sqrt{T_0^2 + w^2 s^2} \tag{3.32}$$

where T_0 is the bottom tension and s is the length of the catenary line. At zero bottom tension, the catenary length becomes $s = D$ and the equation reduces to $T = w \cdot D$.

[12]The expression "laying wheel" stands here also for a laying chute or similar overboarding arrangements.

A complete mathematical treatment of the catenary line is given in the appendix to Chap. 7.

The vertical movement of the laying sheave caused by wave-induced vessel motion adds a dynamic force to the weight of the cable in the catenary line. We assume that the vertical movement of the laying sheave is sinusoidal and find the maximum vertical acceleration $b_{\max}$:

$$b_{\max} = h/2 \cdot (2\pi/P)^2 \tag{3.33}$$

where h is the vertical movement amplitude (measured peak to peak) and P is the movement period (time between subsequent wave peaks). The maximum force on the hanging cable is now

$$T_{\max} = T_s + m \cdot b_{\max} \tag{3.34}$$

where m is the mass of the hanging cable. Since the force due to acceleration is an inertia phenomenon, the cable mass must be used for the calculation rather than the weight in water or air. Each cable laying ship has different sea-keeping characteristics describing how the vessel reacts on different waves from different directions. What matters for the cable top tension, is the vertical acceleration of the laying wheel. Predominantly pitch and heave movements influence the wheel vertical movements. A more detailed treatment of wave statistics and the relation between wave movement and wheel movement is given in Chap. 7.

Real waves sometimes do not obey the sinus equation. Instead, they are, in parts of the wave silhouette, steeper than a sinus curve. In other cases, waves from different directions and different causes can be superimposed, which leads to very steep wave fronts. In these cases the vertical acceleration $b_{\max}$ and hence the dynamic forces may be substantially larger than indicated by the sinus calculation.

The tensional forces on the cable are results of waves with a statistically distributed wave height. Even if the significant wave height of the weather forecast seems to be acceptable, a few waves of exceptional amplitude can cause tensions big enough to damage the cable. The installation engineer must always keep this in mind.

It is evident that the simple sinus representation of the vessel movement is sometimes not adequate to describe statistically rare events. To take into account even unexpected events, guidelines for cargo stowing recommend lashing dimensions fit for vertical acceleration of up to 1 g (=9.81 ms^{-2}) at the aft and bow of a vessel ([9], in Chap. 7). If no detailed values about the cable ship's vertical movements are known, a value of $b_{\max} = 6\ ms^{-2}$ shall be assumed.

It is rather easy to estimate the contribution of the catenary and the wave dynamics to the top tension separately. The results give us an idea on the augmentation of the tensional forces due to both effects. It is much more complex to calculate the combined effects on the tensional forces of a catenary line and the vertical acceleration dynamic.

The entire length of the suspended catenary, also the cable portion close to the TD, must be accelerated vertically. However, the inclined cable can transmit forces only in its own axial direction. For this reason, large tensions along the cable have to be transmitted to create the vertical forces for the cable acceleration close to the TD. A complete laying analysis with resulting tensional and bottom tension values can be performed with specialised commercial software. Some of the software tools also can take the vessel's response to various sea-states into account. Engineering companies working for the offshore industry, and submarine installation companies, often have such tools.

It is a straight-forward task to design the armoring of a submarine power cable for the tensional forces in a catenary line in calm weather. It is more difficult to determine for which sea state the cable should be designed during installation. The selection of the maximum considered sea-state is a matter of attitude rather than engineering. The sea-state statistics for the installation area and the intended installation season can be found out in a desktop study. It must subsequently be decided which range of sea-states the cable should be designed for. If the cable is designed only for the stresses occurring in moderate sea-states, the number of suitable weather windows for installation will be small. If the cable design allows for higher sea-states during installation, more and longer laying opportunities will appear. The costly risk that a laying operation has to be terminated due to adverse weather is reduced.

3.2.2 The Cigré Test Recommendation

The only known mechanical test recommendation for submarine power cables is the Cigré test recommendation for submarine cables [15], referred to as Electra 171 in the following. The most prominent test of the recommendation involves simultaneous bending and pulling of the cable, resembling the stress during pay- out of the cable over the laying wheel. The test arrangement is shown in Fig. 5.9 in Chap. 5. Electra 171 suggests tension values as follows (cf. Fig. 3.10):

For a laying depth up to 500 m:

$$T = 1{,}3 \cdot w \cdot d + H \cdot \tag{3.35}$$

where w and d are as explained above. The additional force H reflects the bottom tension of the cable during installation. H is:

$$H = 0{,}2 \cdot w \cdot d_1 \tag{3.36}$$

with d_1 being the laying depth but 200 m at minimum.

For depth greater than 500 m, Electra 171 suggests another tensional force:

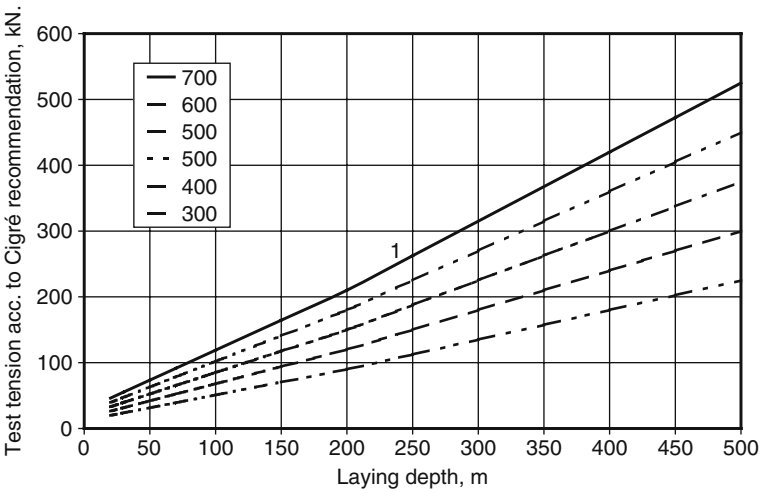

Fig. 3.10 Tensional force for testing according to the Cigré recommendation. The curve parameter is the weight of the cable in water (N/m)

$$T = 1{,}3 \cdot w \cdot d + H + 1{,}2 \cdot |D| \tag{3.37}$$

where $|D|$ represents the dynamic tensions (in N) calculated as:

$$D = \pm {}^{1}/_{2} \cdot b_h \cdot m \cdot d \cdot \varpi^2 \tag{3.38}$$

b_h the vertical movement, crest to crest, of the laying wheel
m mass of cable in air, kg/m
ϖ $2\pi/t$, circular frequency of the vertical movement of the laying wheel, 1/s
t movement period, in seconds.

This formula does not take into account the cable catenary shape but reflects simply the inertial force of the hanging cable under the acceleration during ship movements.

The Electra 171 test values cover most cases of submarine laying operations. In tough weather conditions, however, the resulting tensional forces can be substantially higher. Table 3.9 illustrates this for a typical single core 1200 mm^2 extruded HVDC cable. While the Electra 171 test value is 78 kN, expected values in tough weather can reach 106 kN. This value still does not include any allowances for the dynamic forces in the catenary nor any safety margins. With sinusoidal wave shapes a vertical acceleration of 6 ms^{-2} occurs under quite rough sea-states only. However, irregular wave shapes and interfering waves can generate vertical acceleration of this size in the laying wheel at the stern of the vessel.

Table 3.9 Comparison of tensional test values of Electra 171 and estimated maximum tensional forces in heavy weather

Mass of the cable	29 kg/m
Weight in water	209 N/m
Laying depth	250 m
Force attributed to bottom tension (H in Eq. 3.35)	10.450 N
Static force $w{\cdot}d$	52.250 N
Tensional test force according to Electra 171 (Eq. 3.35)	78.375 N
Assumed vertical acceleration $b_{\max}$	6 ms^{-2}
Dynamic force $m{\cdot}b_{\max}$	43.500 N
Total tensional force $T{=}\ w{\cdot}d{+}\ m{\cdot}b_{\max}{+}H$	106.200 N

3.2.3 Distribution of Mechanical Stress Between Conductor and Armoring

In the following, the response of a single-core DWA submarine cable with steel armoring and copper conductor is discussed. The equations can easily be adapted to other armoring and/or conductor materials. When a tension is applied on the cable the elongation and the tensions in the armor wires and the conductor is given by

$$\varepsilon = \frac{F_A}{E_A \cdot A_A} = \frac{F_L}{E_L \cdot A_L} \tag{3.39}$$

$$F = F_A + F_L \tag{3.40}$$

where

F Total tension (N)
F_A Tension in the armoring (N)
F_L Tension in the conductor (N)
E_A Young's modulus of steel (N/mm^2)
E_L Young's modulus of the copper conductor (N/mm^2)
A_A Total cross section of the armoring wires (mm^2)
A_L Conductor cross section (mm^2).

The tension in the conductor can be calculated as follows:

$$\frac{F - F_L}{E_A \cdot A_A} = \frac{F_L}{E_L \cdot A_L} \Rightarrow F_L \left(1 + \frac{E_L \cdot A_L}{E_A \cdot A_A}\right) = F \cdot \frac{E_L \cdot A_L}{E_A \cdot A_A} \Rightarrow$$

$$F_L = \frac{E_L \cdot A_L}{E_A \cdot A_A + E_L \cdot A_L} \cdot F \tag{3.41}$$

The conductor stress σ_L is as follows:

$$\sigma_L = \frac{E_L \cdot A_L}{A_L \left(E_A \cdot A_A + E_L \cdot A_L\right)} \cdot F \tag{3.42}$$

The tension in the armoring wires is:

$$F_A = F - F_L \Rightarrow F_A = F \cdot \left(1 - \frac{E_L \cdot A_L}{E_A \cdot A_A + E_L \cdot A_L}\right) \tag{3.43}$$

The total armoring tension is divided between the inner armoring layer (F_{AI}) and the outer armoring layer (F_{AO}):

$$F_A = F_{AI} + F_{AO} \tag{3.44}$$

$$\frac{F_{AI}}{F_{AO}} = \frac{A_{AI} \cdot E_A}{A_{AO} \cdot E_A} \tag{3.45}$$

where

A_{AI} Total cross section of the inner layer (mm^2)
A_{AO} Total cross section of the outer layer (mm^2).

Now the tension in the inner and the outer armoring layer can be calculated from Eqs. 3.43, 3.44, and 3.45:

$$F_{AO} = F \cdot \frac{A_{AO}}{A_{AO} + A_{AI}} \cdot \left(1 - \frac{E_L \cdot A_L}{E_A \cdot A_A + E_L \cdot A_L}\right) \tag{3.46}$$

$$F_{AI} = F \cdot \frac{A_{AI}}{A_{AO} + A_{AI}} \cdot \left(1 - \frac{E_L \cdot A_L}{E_A \cdot A_A + E_L \cdot A_L}\right) \tag{3.47}$$

Finally, the mechanical stress in the inner (σ_{AI}) and outer (σ_{AO}) armoring layer is:

$$\sigma_{AO} = \frac{F}{A_{AO} \cdot \cos\varphi_O} \cdot \frac{A_{AY}}{A_{AO} + A_{AI}} \cdot \left(1 - \frac{E_L \cdot A_L}{E_A \cdot A_A + E_L \cdot A_L}\right) \tag{3.48}$$

$$\sigma_{AI} = \frac{F}{A_{AI} \cdot \cos\varphi_I} \cdot \frac{A_{AI}}{A_{AO} + A_{AI}} \cdot \left(1 - \frac{E_L \cdot A_L}{E_A \cdot A_A + E_L \cdot A_L}\right) \tag{3.49}$$

φ_O is the lay angle of the outer layer (in degrees)
φ_I is the lay angle of the inner layer (in degrees).

For many submarine cable projects, in particular in shallow waters, an armoring with thin wires would be sufficient to comply with the tensional bending test according to Electra 171. However, as the maximum number of wires that can be handled in the armoring machine in one run is limited, manufacturers often use thicker wires to achieve a complete coverage of the cable circumference. In doing so, the cable is

Table 3.10 Guide values for mechanical properties of copper and steel. Steel grade values from European Standard EN 10257-2:1998

Wire material	Breaking stress (N/mm^2)	Yield point (N/mm^2)
Copper wire	220–240	120
Copper wire – welding zone	170–210	70–80
Mild steel (grade 34)	340 . . . 540	min 210
Steel grade 65	650 . . . 850	
Steel grade 85	850 . . . 1050	
Steel grade 105	1050 . . . 1250	
Steel grade 125	1250 . . . 1450	

equipped with a stronger armoring than the Electra 171 test would require. But the additional steel also provides additional lateral protection, a property much needed in certain projects as the next chapter explains.

In cases where the additional protection of an oversized armoring is not necessary or wanted, some of the steel wires may be replaced by plastic filler wires. This reduces weight, magnetic losses, and possibly costs.

The armoring wire length is longer than the power cable length. Table 3.11 gives the overlength as a function of the lay-length.

One should not conclude that a long lay-length (20 or 25 times the diameter) would save material because of the short overlength in Table 3.11. A long lay-length simply requires more wires to cover the complete cable circumference.

Table 3.11 Armoring wire overlength as a function of the lay-length

Lay-length as multiple of the diameter of the armoring layer	Ratio of armoring wire length to cable length
10	1.048
15	1.022
17.5	1.017
20	1.012
25	1.008

3.2.4 Other Forces and Impacts

The armoring must withstand all forces that can be reasonably expected during installation and operation. The tensional forces that occur during installation can be predicted with a certain degree of accuracy. Other forces and impacts during installation and operation have an accidental nature and hence are indifferent in their character, amplitude and frequency. Many types of external forces and stresses might attack the cable during installation and/or operation:

- Overbending, mostly during installation because of inadequate equipment or insufficient control
- Impact from edges or rocks may happen during burial operations
- Squeezing from cable engines or inadequate roller arrangements
- Impacts from anchors and fishing tackle.

It is difficult to quantify the magnitude of external violence from the accidental events listed here. The design of cable armoring should be based on a compilation of the expected dangers and threats along the cable route, including the hazards arising during the installation. The history and experience from previous submarine cable installations is another valuable source of knowledge. Unfortunately there is no general design rule for the thickness and number of the armoring wires because impacts, threats, and peak tensions are statistic events. Most manufacturers consider the design data as property, not suitable for publishing. Still, there are a few self-evident rules of thumb:

- more steel provides better protection
- harder wires provide a better protection
- double wire armoring is tougher than single wire armoring
- a short-lay rock armoring provides a better protection against lateral impacts at the expense of tensional force.

The optimum armoring wire thickness is depending on several factors. First of all there must be a minimum wire thickness to withstand the external threats such as fishing gear and anchors. On the other hand, most cable manufacturers can apply only a limited number of wires onto the cable. In order to reach a complete cover of wire armoring they must apply thick dimensions of wire for a complete coverage. The thickness of the armoring wires has a large impact on both weight and diameter of the cable. Hence, the cable length in each shipload and the laying schedule are influenced noticeably by the wire thickness.

The American standard ICEA No. S-57-401/NEMA Standards Publication No. WC2 determines the required wire thickness for paper-insulated submarine cables

Table 3.12 Thickness of armoring wires according to US standard

Calculated diameter of cable under the armoring bedding mm	Size of armoring wires, mild galvanized steel BWG	mm
0–19.05	12	2.77
19.08–25.40	10	3.40
25.43–43.18	8	4.19
43.21–63.50	6	5.16
63.53 and larger	4	6.05

according to Table 3.12. However, the standard does not tell if this is valid for single or double-layer armoring, or both.

The side-wall pressure impact (SWP) value is often required to know for the planning of the installation. Literally, SWP is the maximum allowed lateral squeezing force, which the cable can stand without serious damage. The name SW-pressure is misleading as it describes a force per unit length (N/m) rather than a pressure (N/m^2). The SWP can best be described as the lateral force onto a cable, which is bent around a wheel under a tensional force. SWP can be expressed by:

$$SWP = F_T/R \tag{3.50}$$

where F is the pulling force and R the wheel or bend radius. There are no literature values for the maximum permissible SWP of submarine power cables. However, for some cable projects the tensional force used during tensional bending tests have been reported. The results are summarized in Table 3.13.

Table 3.13 SWP in some cable projects

Link	Armoring	Insulation	Test tension kN	SWP kN/m	References
Morocco – Spain	DWA copper	LPOF	353	70.6	[16]
Italy – Greece	DWA steel	MI	471	94.2	[16]
Gulf of Aqaba	DWA	LPOF	500	100	[17]
Troll A	DWA	Dc XLPE	375	75	

It is expected that double-wire armored cables have a substantially higher permissible SWP than single-wire armored cables. A short-lay rock armoring provides probably even higher SWP.

It must be kept in mind that the SWP refers to a distributed lateral force on the cable. The effects of concentrated impacts or lateral forces cannot be treated with the concept of SWP.

Submarine cable producers often are asked for data on the bending stiffness of submarine power cables. A critical parameter for bending stiffness calculations for cables is the friction between the cable layers. Submarine cables are constructed from a variety of different materials. Friction data are known only with limited accuracy, in particular the friction in the armoring layers. For the steel wire armoring layer, coated to a certain extend with bitumen, a complicated mixture of static and dynamic friction coefficients is applicable. Furthermore, the friction and hence the bending stiffness, is strongly depending on the temperature, which influences the bitumen properties, and the amplitude and radius of the bending. For this reason, technical data on the bending stiffness of submarine power cables of standard design are prone to large inaccuracies. The bending stiffness has no influence on the value of the top tension during laying, but can critically change the bending radius at the TD when the laying wheel moves down in heaving.

A few examples of armored cables and their fate might be interesting to know about:

Two mass-impregnated HVDC cables were installed between Denmark and Norway in the mid-70ties. After full-size tests of the resistance of the cable against external aggression, it was equipped with two layers of armoring, 7.0 and 5.6 mm thick, respectively. These cables were put out of service by very heavy fishing gear in 1976 and 1977, and by a dragged towing weight in 1981 [18]. Until 1984, the cables survived the hits from about 30 anchors and fishing trawls which had got entangled with the cables in waters between 160 and 300 m.

The Baltic Cable with two layers 5.0 mm steel wire armoring did survive some violent anchor entanglements but was damaged seriously by the ferryboat "Nils Holgersson" that lost rudder control outside Travemünde/Germany and hit ground and cable. Another outage was caused by an emergency anchoring. At another incident, the cable survived the encounter with a heavy anchor.

Another submarine power cable with two layers of 6.3 mm wires was damaged during the trenching operation, probably by an unsuitable trenching plough.

The notorious Fox Islands Cables between Rockport, Maine, and the islands of North Haven and Vinalhaven, which suffered a large number of mechanical faults (due to anchors, fishing gear, mistreatment during installation and repair, and unsuitable installation over a steep seafloor outcrop) had #4 BWG galvanized wires (=6.054 mm).

3.2.5 Vortex Induced Vibrations

Irregular seafloors and steep underwater slopes can cause free spans of the cable. Submarine cables hanging in free spans are exposed to oscillations when water currents strike them. The water current creates Karmán-vortices, which separate from the cable alternating on the upper and the lower "edge" of the cable. Such vortices can also be observed in the wake of bridge posts in a streaming river. The dispersal of vortices from the cable is called vortex shedding. Each time a vortex is leaving the cable, a force is exerted on the cable. If the cable is horizontal and the water current also is horizontal but perpendicular to the cable, the forces from the vortex shedding point vertically alternatively up and down. The frequency (Hz) of the vortex shedding is

$$f_s = St\frac{u}{D} \tag{3.51}$$

with f_s the vortex shedding frequency (Hz), u the velocity of the streaming water (m/s), D the diameter of the cable (m), and St the Strouhal number [19]. For submarine power cables and relevant current velocities St can be assumed 0.2.

A cable hanging in a free span has a number of natural frequencies with which it can vibrate like a guitar string. The natural frequencies f_n are multiples of the basic natural frequency:

$$f_n = \frac{n}{2} \cdot \sqrt{\frac{T_a}{m' \cdot L^2}} \tag{3.52}$$

Table 3.14 Basic natural frequency and minimum flow velocity for the establishment of VIV

Cable span data	Large cable	Small cable
Cable mass per meter, kg/m	40	20
Length of free span, m	20	40
Tension in the span, kN	10	2
Cable diameter, mm	110	80
Frequency of the basic natural frequency, Hz	0.40	0.125
$V_{\min}$, m/s	0.22	0.05

with n the mode number, T_a the tension of the cable, m' the mass per length unit of the cable, and L the length of the free span [20].

The cable in free span is excited by the force from the leaving Karmán vortices with an oscillating frequncy f_s. When the exciting frequency f_s is close or equal to one of the natural frequencies f_n the cable may start vibrating in resonance. This phenomenon is called "lock-in". Combining Eqs. 3.51 and 3.52 results in a minimum flow velocity for the lock-in and the establishement of vibrations:

$$u_{\min} = \frac{D}{2 \cdot St} \cdot \sqrt{\frac{T_a}{m' \cdot L^2}} \tag{3.53}$$

According to [20], this simple relation can be used to make a first assessment of the risk for vortex-induced vibrations (VIV) in a given cable installation situation. Table 3.14 shows the calculated results for two typical cable designs.

It should be noted that the diameter of the cable could change drastically by marine growth. The density of marine growth may be set to 1325 kg/m^3. If site-specific information is not available the thickness of marine growth can be assumed as indicated in Table 3.15.

As soon as the cable starts vibrating, its natural frequencies are changed. This is partly due to the inertial force of the water, which is pushed by the moving cable. In hydrodynamics, this is addressed by the added-mass coefficient describing a virtual increase of the mass of the accelerating cable due to the dense medium around it (the water). The added-mass coefficient decreases the natural frequencies, more for cables with low own density (such as aluminium cables or three-phase cables) but only little for cables with high density (such as single-core copper cables). Furthermore, the added-mass coefficient is depending on the actual flow velocity [19].

Table 3.15 Thickness of marine growth on submarine structures [19]

	Latitude	
	56–59° N	59–72° N
Water depth	Thickness of marine growth (mm)	
+2 . . . –40 m	100	60
Below –40 m	50	30

The bending stiffness of the cable may change the natural frequency to higher values. The influence of the bending stiffness can be estimated from the value φ:

$$\varphi = \left(\frac{n\pi}{L}\right)^2 \cdot \frac{E \cdot I}{T_a} \tag{3.54}$$

where $E{\cdot}I$ is the dynamic bending stiffness of the cable. If $\varphi << 1$, the influence of the bending stiffness can be neglected [20].

Once lock-in has established, the vortex shedding frequency is dictated by the actual oscillating frequency of the cable rather than Eq. 3.51.

In long spans, the higher order natural frequencies lie close together. A certain vortex shedding frequency f_s with its associated bandwidth can strike excitation of many natural frequencies or modes simultaneously. However, as the energy included in each mode is small the risk for lock-in is reduced.

An additional complication arises when the flow speed is not uniform along the span of the cable. The response of cables on non-uniform flow fields has been described e.g. in [21, 22]. In the first place, project planners should try to avoid free spans by any means such as route diverting or seafloor leveling.

Some design changes can contribute to reduce the risk of VIV. The cable mass per meter can be changed by a thicker lead sheath, or, in case of three-phase cables, by lead profiles in the interstices between the cable cores [23]. Increased mass-per-length reduces the cable's natural frequency and the minimum necessary flow velocity, but can also reduce the amplitude of the oscillation. VIV suppression strakes can be mounted onto the cable to break up the laminar flow necessary for the vortex creation and shedding. The severity of a given installation situation can be assessed with commercial software packages in use in the offshore oil and gas industry. Reference [19] provides a comprehensive bibliography on the subject.

3.3 Electric Design

The electric design of submarine power cables follows the same design principles as those for underground cables. Since submarine cables are often more remote and less accessible for repair, it should be considered to increase the safety margins. The task of this chapter is not to repeat the well-documented principles of the electric design of a.c. power cable [1, 23, 24]. Instead, a very short overview is presented. A little more attention is dedicated to the dielectric properties of d.c. submarine cables as these have not been treated in reference literature to the same extent.

3.3.1 The Concept of Electric Strength

The electric strength of an insulation material is the ability to withstand an applied voltage without a breakdown. If the voltage is higher than the electric strength, an electric breakdown occurs. No matter which mechanism initiates the breakdown, the

result is a sudden discharge of the voltage through the insulation. In cable insulation, such an event inevitably leads to a complete failure and an outage of the power line. The cable insulation must be designed such that it can withstand all expected voltages during the lifetime of the cable.

The electric strength is a material property given in kV/mm. There are no fixed values for solid insulation materials, even if tables with electric strength values can be found in many textbooks and journal articles. The electric strength of a given material is depending on a number of parameters under which the electric strength has been measured. Sometimes, the concept of "intrinsic dielectric strength" of a material is used. The expression describes the electric strength of an ultra-pure sample in a laboratory without any deteriorating influences. The published "intrinsic dielectric strength" values of insulation materials are many hundred kV/mm. Those experiments are conducted on very thin layers of insulating material between extremely smooth electrodes. The electric strength of insulation material depends on the volume of the stressed dielectric. Even if the breakdown voltage of a thick layer of insulation material is higher than that of a thin layer, the dielectric strength as expressed in kV/mm is usually smaller. The reason for this is the increased number of impurities and other irregularities in a thick insulation layer compared to a thin layer. These irregularities can act as starting points for a breakdown. For this reason, the electric strength in industrial insulation systems, such as cables, is usually one or two orders of magnitude lower than those that can be achieved in small laboratory materials samples.

Furthermore, the actual dielectric strength is depending on temperature, voltage shape and duration, ageing etc. All these factors should be considered when consulting tabulated dielectric strength values for the electric cable design.

3.3.2 The Weibull Distribution

Electric breakdown is a statistic process. Repeating the same experiment with equal samples and test conditions will result in a statistic distribution of results. The Weibull distribution is widely used to describe the results of electric breakdown experiments. The 2-parameter Weibull distribution can be expressed as:

$$f(E) = \frac{\beta}{\eta}\left(\frac{E}{\eta}\right)^{\beta-1} e^{-\left(\frac{E}{\eta}\right)\beta} \tag{3.55}$$

where *f(E)* is the probability that the sample suffers a breakdown under the application of the electric stress *E*. η is called the scale parameter and β the shape parameter of the Weibull distribution. Very interesting is the accumulated probability F(E) for a breakdown:

$$F(E) = 1 - e^{-\left(\frac{E}{\eta}\right)\beta} \tag{3.56}$$

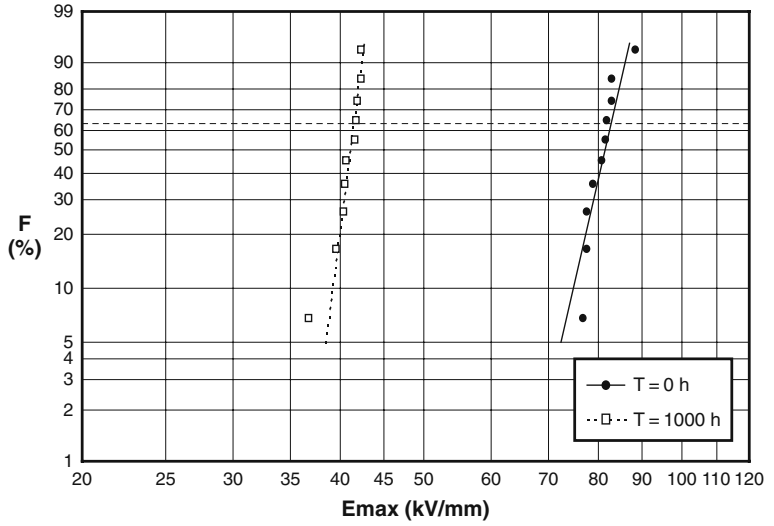

Fig. 3.11 Results of breakdown experiments plotted on Weibull paper. Explanation in the text (Courtesy of Borealis, Sweden)

For a group of samples, *F(E)* returns how many of these samples will have failed when tested with an increasing electric stress up to *E*. Figure 3.11 shows a Weibull plot of two experiments with insulation material. The test electric stress is on the x-axis, and the probability of failure is on the y-axis. Plotted on "Weibull paper" with its particular axis formation, Weibull-distributed experimental data should lie on a straight line. From the Weibull plot of experimental data, the scale parameter η and the shape parameter β can be determined. The scale parameter η in Eqs. 3.55 and 3.56 can be interpreted as a measure for the dielectric strength of the material under the given test conditions. The shape parameter β tells us something about the statistical scatter of breakdown values over the electric stress scale. A high β value indicates a material where the most samples fail within a narrow range of electric stress. A small β value indicates a material where samples fail within a large range of stress values. Such a material seems to be less predictable.

The Weibull plot can be used to compare an insulation material in different ageing stages, or different insulation materials. In Fig. 3.11, two sets of breakdown data are plotted into the same diagram. The solid dots represent the results of breakdown experiments on fresh material, while the open dots result from tests on aged material. In spite of the scatter of breakdown voltage as a result of the statistic nature of electric breakdown, it can be seen clearly that the material represented on the right side of the diagram performs better than the left material [25].

Weibull can do more than this. In Eq. 3.56, the variable is the electric stress *E* and the Weibull distribution describes the failure probability with respect to the applied electric stress. The Weibull statistics can also be used to assess the influence of other parameters on the breakdown behaviour of insulation materials. It is known

that the breakdown strength is depending on temperature and the duration of applied voltage. Experiments can be carried out where the breakdown probability is tested as a function of temperature at constant electric stress. The distribution is expected to follow Eq. 3.56 with temperature θ substituted for the electric stress:

$$F(\Theta) = 1 - e^{-\left(\frac{\theta}{\eta}\right)\beta} \tag{3.57}$$

In this case, *F(θ)* describes the accumulated risk of failure for breakdown experiments at temperature θ. The parametersη and β of this Weibull distribution are naturally different from those for the stress-related Weibull distribution in Eq. 3.56. The parameters can only be established by experiment.

In a similar way, the basic Eq. 3.56 can be used to describe how the electric strength of insulation material depends on the duration of applied electric stress. If E in Eq. 3.56 is substituted with the time duration T of applied voltage, a statistical analysis of the influence of time on the electric strength can be made.

$$F(T) = 1 - e^{-\left(\frac{T}{\eta}\right)\beta} \tag{3.58}$$

Again, *F(T)* describes the probability that a sample fails before or at the time T of voltage exposure. This probability distribution is valid for a certain experiment set-up in terms of temperature, voltage, electrode shape, etc. And again, the parametersη and β of this Weibull distribution are different from those for the stress-related Weibull distribution in Eq. 3.56.

A utility operating a network of identical cables can plot the cables' lifetime in a Weibull diagram to evaluate the scale parameter η and the shape parameter β. From this evaluation, the mean-time-to-failure (MTTF) of a new cable circuit can be calculated:

$$\bar{T} = \eta \cdot \Gamma\left(\frac{1}{\beta} + 1\right) \tag{3.59}$$

where Γ is the gamma function evaluated at $(1/\beta + 1)$. The shape parameter β can help to estimate if all cables in a circuit will fail approximately during a few years around the MTTF, or if the failures (and repair costs) will be scattered over a longer time period. However, the empirical evaluation of η and β from the failure data of installed cables is very difficult and probably unreliable. The operation data of the cables such as temperature, magnitude, and duration of overvoltages etc., use to differ so much that no homogeneous cable population can be found for the statistics.

The application of Weibull statistics for power cables is described in detail in [26]. The reference also contains a bibliography on the subject.

Relevant lifetime tests can be made in the laboratory with elevated voltage. The evaluation makes use of the fact that applied stress and lifetime are related:

$$(V - V_0)^n \cdot t = \text{const.} \tag{3.60}$$

where V is the applied voltage (representative for the electric stress, which easily can be deducted from V), V_0 is a threshold value, and t is the time to failure. The exponent n is a material constant. Test samples from laboratory tests performed under controlled conditions are suitable for statistical treatment [27].

Experimental data can be plotted into a Weibull diagram in order to assess different insulation materials. The Weibull distribution is a valuable tool for researchers to compare different insulation materials in terms of electric strength.

3.3.3 Dielectric Design of a.c. Cables

While the thermal design of a.c. cables is a complex matter due to the extra losses generated by the alternating magnetic field, the electric design of a.c. submarine power cables is so much easier. The cable insulation must be designed in such a manner that the electric stress caused by all expected voltages in the cable system do not exceed the breakdown strength of the insulation, allowing for a safe margin also after reasonable ageing of the insulation.

For a.c. and transient voltages, the stress distribution in the insulation is capacitive. It can be calculated using the Laplace equation $\nabla^2 \Phi = 0$ for space-charge free dielectrica, where ∇^2 is the Laplace operator and Φ the electric potential. In cables, cylindrical coordinates are useful. The Laplacian operator ∇^2 applied to the function f reads in cylindrical coordinates:

$$\nabla^2 f = \frac{1}{r}\frac{\partial}{\partial r}\left(r\frac{\partial f}{\partial r}\right) + \frac{1}{r^2}\frac{\partial^2 f}{\partial \theta^2} + \frac{\partial^2 f}{\partial z^2} \tag{3.61}$$

For the axi-symmetric case of a cable insulation the two last terms of the right side of Eq. 3.61 vanish. After integration of the remaining equation and proper setting of the boundary conditions the electric stress in the a.c. cable insulation can be expressed as:

$$E(r) = \frac{U}{r \ln\left(D_o / D_i\right)} \tag{3.62}$$

with the following symbols:

U applied voltage
r radius in the insulation
D_o Outer diameter of the insulation = insulation diameter under the insulation screen
D_i Inner diameter of the insulation = diameter over the conductor screen.

The applied voltage in Eq. 3.62 is the phase-to-ground voltage $U_0 = U_r/\sqrt{3}$ where U_r is the phase-to-phase system voltage. The stress distribution in the insulation of

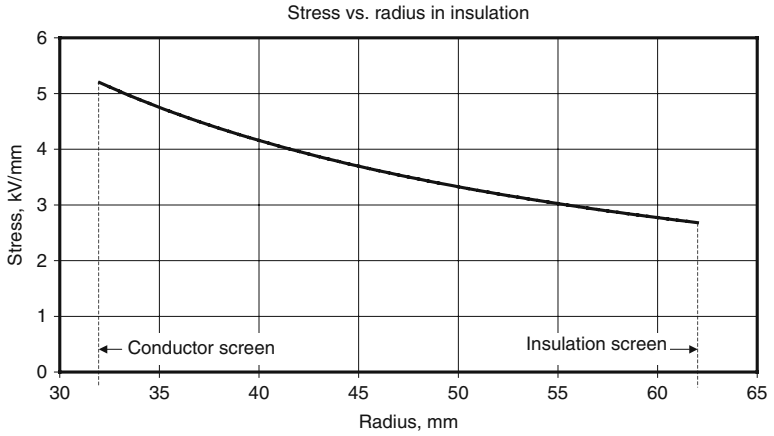

Fig. 3.12 Electric stress in a 110 kV a.c. XLPE cable

a 110 kV 630 mm^2 XLPE cable is shown in Fig. 3.12. The 15 mm insulation wall has $D_o = 62$ mm and $D_i = 32$ mm.

The stress distribution given in Eq. 3.62 and Fig. 3.12 postulates that the relative dielectric constantε_r has the same value in the entire insulation.ε_r is practically independent on temperature and power frequency. Hence the stress distribution formula 3.62 is valid for all a.c. cables, no matter if it is a three-core cable, a single core cable, cold or loaded.[13] The concentration of electric stress at the conductor screen imposes high requirements on material cleanliness and a smooth interface without defects.

Equation 3.62 is also valid for the calculation of stresses under transient voltages such as lightning or switching impulses but must not be used for the calculation of stresses in d.c. cables.

Equation 3.62 can also be used to determine the required insulation thickness for the cable to withstand the expected voltages. The crucial task is to establish the highest acceptable stress for power frequency voltage, switching impulse and lightning impulse taking into account system overvoltages.

3.3.3.1 Overvoltages

During testing and operation of submarine power cables a number of different voltage shapes can occur. Power frequency overvoltages can occur during a single-phase-to-ground cable failure until the fault is cleared. Depending on the system earthing concept, the overvoltage over the insulation of the healthy phases can be

[13]Only some low-voltage cables without insulation screens maintain non-circular stress distributions.

3 times the rated phase-to-ground voltage. This overvoltage, though not very long lasting, can result in extra ageing or even breakdown.

Other overvoltages can be caused by abnormal operation conditions such as incorrect generation/load balance, especially when the submarine cable is used to connect a remote isolated load or generator to the shore grid. A detailed system study can clarify the expected overvoltages in the particular project, and suggest suitable protection measures.

With respect to the strong correlation between overvoltages and ageing, it should be avoided to operate submarine power cables at the maximum design voltage U_m during the greater part of the operational time.

Voltage impulses with high magnitude and very short duration may occur in power transmission systems as a result of switching operations and atmospheric lightning. The duration of these voltage peaks is in the range of micro- or a few milliseconds. The electric stress in the insulation during impulse voltages can be calculated using Eq. 3.62. Fortunately, the dielectric strength of insulation materials under impulse stress is much higher than under power frequency voltage.

Test standards recommend test voltage level for Lightning Impulse tests (LIWL) and Switching Impulse tests (SIWL), cf. Table 3.17. Test levels for a.c. routine tests are summarized in Table 5.5.

3.3.3.2 Design Rules

Scientific books and research articles can provide dielectric strength values for different materials and experimental conditions but they can hardly provide design rules. In addition to laboratory results, the experience and safety policy of power utilities influence the selection of safety factors for the dielectric cable design. National or international standard committees, power utilities and each cable manufacturer have developed own attitudes concerning safety factors and design rules. Given the "minority" role of submarine power cables compared to land-based power cables, almost all cable standards refer to underground cables, leaving the field of submarine cables with little regulation.

The USA industrial standard AEIC CS9-06 lists maximum stress values and the corresponding insulation thickness (Table 3.16)

The European International Electric Commission (IEC) does not recommend any particular insulation wall thickness for high-voltage cables. Instead, test procedures both for power frequency and impulse withstand tests are specified, and a cable design is approved if the relevant type tests are passed (cf. Chap. 5).

Power utilities may have their own cable design standards. Major German TSO's have agreed on a common standard for the insulation thickness of 110 kV XLPE cables: 18 mm. Most cable manufacturers would support a thinner insulation such as 15 mm.

For medium-voltage cables ($\leq$ 36 kV) with an insulation thickness of 4–8 mm, the maximum design stress in the insulation is only between 2 and 4 kV/mm. Modern XLPE insulation has a much higher breakdown strength than this. However, the thin insulation wall renders this insulation more sensitive to production irreg-

Table 3.16 Stress limits and insulation thickness for extruded cables according to [28]

Rated voltage (kV)	Conductor size, (mm^2)	Nominal internal ac stress limit (KV/mm)	Corresponding generic insulation thickness (mm)
69 wet	240–2000	4	16.5
69 dry	240–2000	6	12.0
115	400–2000	8	15.0
138	400–2000	8	18.0
161	400–2000	9	20.0
230	500–2500	11	23.0
345	500–2500	14	26.0

Note. The nominal internal stress is the electric stress at the conductor screen at rated phase-to-ground voltage. A "wet" design is a cable without impermeable metallic sheath. The limits given in the standard are valid unless proposed otherwise by the manufacturer or purchaser.

ularities. Higher design stress and thinner insulation would be possible but would require a more definite and costly production and the use of higher grades of insulation material.

For higher rated cables ($\geq$ 150 kV), higher design stresses are generally accepted as a result of better polymer grades and a higher relative thickness stability of the insulation. This can be achieved despite the fact that the specific breakdown strength in thicker XLPE layers is lower than in thin XLPE layers [29].

3.3.4 Dielectric Design of d.c. Cables

Direct current high-voltage power transmission is more than a century old, and paper-insulated submarine cables have been used for submarine d.c. transmission since more than 50 years [30]. Extruded d.c. cables have been introduced commercially more than a decade ago by ABB and are now used as submarine cables in a large scale. The increasing need for long-haul submarine power transmission fuels a large interest in the properties of d.c. cable insulation materials.

The d.c. voltage of normal operation creates a field distribution in the cable dielectric that is controlled by the specific conductivity σ of the insulation material. The specific conductivity $\sigma = \sigma(E, T)$ is a function of local electric field and temperature. For this reason, a simple analytic solution of the Laplace equation, as in the case of a.c. cables, cannot be applied.

Various expressions for the dependence on E and T of $\sigma(E, T)$ have been published, such as the following for polymers:

$$\sigma\,(E,T) = A \exp\left(\frac{-\phi \cdot q}{k_B T}\right) \frac{\sinh\,(B\,|E|}{|E|} \tag{3.63}$$

where A and B are constants, ϕ is the thermal activation energy in eV, q is the elementary charge, T the temperature in Kelvins and E the electric field in V/m

[31]. According to other references $\sigma(E, T)$ can be expressed as:

$$\sigma = \sigma_0 \cdot e^{(\alpha(T-273)+\gamma|E|)} \tag{3.64}$$

where σ_0 is the conductivity at 0°C and 0 kV/mm, α is the temperature dependency coefficient, γ is the field dependency coefficient, and E is the local electric field strength [32]. For mass-impregnated cables, we can assume the following:

$$\sigma_0 = 1 \times 10^{-16}\Omega^{-1}\mathrm{m}^{-1}, \quad \alpha = 0.1\,K^{-1}, \quad \gamma = 0.03\,\mathrm{mm/kV}.$$

It is difficult to measure the dependence of σ of E and T as the probes usually need a very long time to stabilize.

Although Eqs. 3.63 and 3.64 are different, they describe two fundamental properties of cylinder-symmetrical d.c. insulation:

1. The higher the electric field at a particular radius r in the insulation, the higher the local conductivity σ(r).
2. The higher the temperature at a particular radius r in the insulation, the higher the local conductivity σ(r).

These properties have far-reaching consequences. Consider a d.c. cable which has just been put under d.c. voltage. In the first instant, the field distribution is according to the green dotted line in Fig. 3.13. The distribution resembles that of an a.c. cable such as shown in Fig. 3.12, with the highest stress at the conductor screen. The relatively high electric field close to the conductor results in a higher specific conductivity in the innermost cylindrical shell of the insulation. As a result, the voltage drop over the shell and the gradient in the same place decrease. After a while, the cold cable d.c. stress distribution has established. This process is called relaxation, and the resulting stress distribution is depicted in Fig. 3.13 as the blue solid line. The distribution represents the situation in a not-loaded cable wich has been under operational d.c. voltage for some hours. The positive effect of the field depending conductivity is to reduce the stress where it is the highest, i.e. next to the conductor. How much the stress peak at the conductor screen is reduced, is depending on the σ(E) function, which is slightly different for different materials.

The next step would be to switch on the current. Once conductor current is flowing, a temperature gradient over the insulation is established, and the situation changes dramatically. As the temperature rises in the insulation close to the conductor, the local conductivity increases further; and this in turn decreases the local stress. The influence of the temperature gradient is much stronger than the influence of the electric field previously was. As a result the stress on the conductor screen decreases considerably, while the stress close to the insulation screen accordingly increases. With large temperature gradients over the cable insulation, the stress profile can actually reverse leaving the cable with the highest stress at the insulation screen. Figure 3.13 shows the electric stress in a d.c. insulation also for full power (red dashed curve) and fully developed thermal gradient.

To describe the d.c. stress distribution the Laplace equation $\nabla^2 \Phi = 0$ of the a.c. distribution is replaced by the more general Poisson equation:

$$\nabla^2 \Phi = \rho \cdot \varepsilon_r$$

where ρ is the local space charge density. Now the insulation layer is no longer space-charge free as in the case of a.c. cable insulation. The transition between the initial transient stress distribution, as depicted by the green dotted line to the no-load d.c. distribution (blue solid) and to the full-load d.c. distribution (red dashed), is associated with the creation and relocation of space charges in the insulation to fulfil Poisson's equation. As space charges have a limited mobility it takes some time to establish a stable stress distribution (a process sometimes called relaxation). The charge mobility is strongly depending on the temperature [33, 34] so that the relaxation speed is different in cold and warm cables. In d.c. submarine cables at 6°C (the seafloor temperature often found in waters in moderate climate zones), it can take many hours to achieve a stable stress distribution. For the design of submarine d.c. cables, it is important to calculate the time-dependant stress distribution under the influence of all expected operational conditions.

The curves of Fig. 3.13 depict the global stress distribution in the d.c. cable insulation. However, this is only a part of the total picture. Many measurements have demonstrated that space charges also accumulate in the immediate vicinity of the dielectric surfaces of the insulation, i.e. close to the extruded conductor screen and close to the extruded insulation screen. These space charges can be caused by charge injection from the semi-conducting surfaces. Sometimes they are homo-charges (same polarity as the neighbouring semi-conductor), sometimes hetero-charges. This space-charge accumulation has led to many failures in the develop-

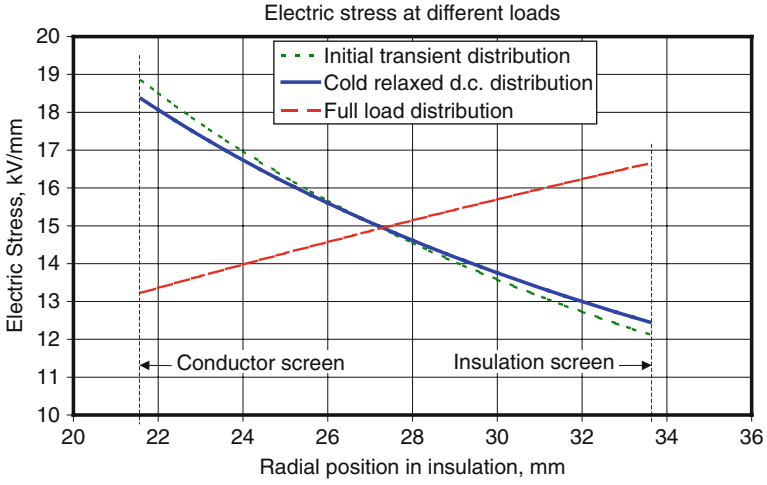

Fig. 3.13 Electric stress in d.c. cable insulation under different load conditions

ment of extruded d.c. cable insulation systems. Only by orchestrated properties of the insulation material and the screen material the problems of space charge related field distortion can be overcome. Today, at least one manufacturer has succeeded and installed more than thousand of kilometres of extruded HVDC cable.

A comprehensive bibliography on space charge phenomenon in polymeric d.c. cables is given in [35].

3.3.5 Dielectric Design of Mass-Impregnated Cables

For practical considerations, the steady-state stress distribution in a mass-impregnated d.c. cable can be calculated analytically according to [36]:

$$\beta = \frac{\alpha \cdot W_C}{2\pi\lambda} \qquad \gamma = \frac{k \cdot U}{r_S - r_C} \qquad \delta = \frac{\beta+\gamma}{\gamma+1}$$

$$E(r) = \frac{\delta \cdot U}{r_S} \cdot \frac{\left(\frac{r}{r_S}\right)^{\delta-1}}{1-\left(\frac{r_c}{r_S}\right)^{\delta}} \quad \text{kV/mm} \tag{3.65}$$

with the following symbols (partly different from [36]):

α [1/K] = conductivity dependence of the temperature
k [mm/kV] = conductivity dependence of the electric stress
U [kV] = voltage conductor – sheath (screen)
r_c [mm] = radius of conductor screen
r_s [mm] = radius of insulation
r [mm] = radius where E is calculated
W_c [W/m] = conductor losses
λ [W/K×m] = thermal conductivity of insulation.

The factor β may also be written:

$$\beta = \frac{\alpha}{2\pi\lambda} \cdot W_C = \frac{\alpha}{2\pi\lambda} \cdot \frac{\Delta\theta \cdot \lambda \cdot 2\pi}{\ln \frac{r_S}{r_C}} = \frac{\alpha \cdot \Delta\theta}{\ln \frac{r_S}{r_C}}$$

The dielectric behaviour of mass-impregnated cables is governed by a particular effect. In contrary to an oil-filled cable, which has an external pressure supply, the mass-impregnate cable has no inner pressure when it is not carrying a load current. Small voids exist in the gaps between the paper tapes, limited in the radial extension by the thickness of the adjacent paper tape. When the cable is loaded with transmission current, the expanding impregnation compound fills up all voids and creates finally an overpressure inside the insulation. Under full load, the dielectric strength of the cable insulation is much higher compared to the no-load situation. For this reason, the cable could be operated at higher voltage under full load conditions compared to no-load conditions. Experience has shown that the dielectric

strength undergoes a minimum during the first one-three hours after reducing the current and, hence, the temperature.

The relevant type tests for mass-impregnated d.c. cables stipulate load cycles with 8 h loading and 16 h cooling ([7], in Chap. 5). The recommended test voltage during the entire load cycle test is $1.8 \times U_0$. According to experience, the cooling phase of the load cycle is the limiting challenge for a given cable design. In practice the mass-impregnated submarine d.c. cable is designed to fulfil the requirements of the Electra 171 type test requirements rather than the challenges of real cable life.

Initially the rated voltage of the tested cable is set such that the cooling phase of the type test will be passed. Doing so, the additional dielectric strength during the full load period cannot be used for real cable operation. In order to utilize the cable in a more economic way, a voltage regulating algorithm has been installed in some HVDC links, which increases the operational voltage on the cable whenever possible using the higher dielectric strength of the insulation under load conditions. The continuous transmission power can be increased by about 25% using this voltage regulation ("CDVC").

Historically, an operational dielectric stress of up to 40 kV/mm has been considered possible for mass-impregnated d.c. insulation [37]. Today, a d.c. design stress of 25–35 kV/mm has been established. The design impulse strength is usually in the range 80–95 kV/mm for impulse tests superimposed on a d.c. voltage with opposite polarity, as stipulated by the Cigré test recommendation. It should be mentioned that the required impulse test levels of mass-impregnated submarine d.c. cables could be lowered noticeable if converter station manufacturers and cable manufactures agreed on closer protection levels for the cable terminations.

3.3.6 Impulse Stress

For all cable types, there are test standards to demonstrate the impulse withstand level. Often, a Switching Impulse Withstand Level (SIWL) and a Lightning Impulse Withstand Level (LIWL) are defined. Table 3.17 lists test levels for LIWL and SIWL

The electric cable cores of submarine power cables are developed and tested according to the same principles as land cables. Therefore, they have to comply with the impulse test requirements given in the applicable land cable standards. Knowing the impulse test voltage, the electric stress in the cable during the test can easily be calculated with Eq. 3.62.

The design impulse stress of power cables can unfortunately not be found in tables. Impulse breakdown voltages are strongly depending on sample size, material purity, manufacturing quality, temperature, electrode structure, etc. Paper insulation tends to have a narrower statistical distribution of breakdown voltage than extruded insulation. For mass-impregnated HVDC cables Electra 189 requires the same peak voltage ($=2.0 \times U_0$) for both Lightning (LI) and Switching Impulse (SI) tests, while the SI test level is lower than the LI level in IEC test standards. In real life, HVDC

Table 3.17 Impulse test levels for a.c. cables

Rated voltage Kv a.c.	Lightning impulse test voltage, kV	Switching impulse test voltage, kV
According to IEC 60840		
20	125	42
30	170	63
45	250	65
66	325	90
110	550	160
132	650	190
150	750	218
220	1050	318
275	1050	400
330	1175	420
400	1425	440
According to British Electricity Boards Engineering Recommendations		
76/132	640	380
160/275	1050	850
230/400	1425	1050

cables of any kind would hardly ever experience overvoltages of the magnitude tested in IEC impulse tests.

Extruded d.c. cables for VSC use are terminated indoors and do not suffer any lightning overvoltage in the classic sense at all. Neither the classic switching overvoltage is experienced for these cables.

3.3.7 Availability and Reliability

The choice of the insulation wall thickness is as much an asset management task as it is an engineering task. Considering the Weibull plots of the cable insulation material, the cable designer will chose an insulation wall thickness which guarantees that the probability of a cable breakdown within the required life time of the cable is below an acceptable level, given the operation temperature and the electric stress on the cable. It must be noted that the statistical risk for breakdown cannot be eliminated completely unless the cable is not being used.

Given the difficulty of submarine cable installations/repairs, it can be prudent to apply conservative design rules for submarine power cables. The large expenses for submarine cable repair might motivate the use of thicker an insulation than it is used for land-based cables, with the purpose of reducing the electric stress and hence the statistic risk of electric failure. On the other hand, experience from submarine power cable operation demonstrates that there are almost no spontaneous electric failures in submarine power cables (cf. Chap. 9).

A thicker insulation would also increase the costs for lead and steel. In the worst case, the larger cable weight and volume would require a larger cable ship or more laying campaigns.

Rather than adding extra insulation the cable should be protected against overvoltage and excess temperature, in order to comply with the rules of thumb (cf. Chap. 2):

- Increase the operating temperature by 8–10°C and you'll cut the lifetime by half.
- Increase the operating voltage by 8–10% and you'll cut the lifetime by half.

References

1. Heinhold L (Ed.) (1990). Power Cables and their Applications, Siemens Aktiengesellschaft 1990, Berlin/Munich, Germany, ISBN 3-8009-1535-9.
2. Anders G J (1997). Rating of Electric Power Cables, IEEE Press, McGraw-Hill, 1997, ISBN 07803-1177-9.
3. Brakelmann H (1985). Belastbarkeiten der Energiekabel, VDE-Verlag, 1985, ISBN 3-8007-1406-X.
4. IEC Standard 60287 (2006). Calculation of the Continuous Current Rating of Cables, International Electrotechnical Commission, Geneva, Switzerland.
5. Neher J H (1964). The Transient Temperature Rise of Buried Cable Systems, IEEE Transactions on Power Apparatus Systems, Vol. PAS-83, pp. 1345–1351.
6. McGrath M H (1964). Discussion Contribution to Neher, IEEE Transactions on Power Apparatus Systems, Vol. PAS-83, p. 113.
7. George F Moore (1997). Electric cables handbook, Blackwell Science, ISBN 9780632040759.
8. Brakelmann H (2004). Bemessung der Energiekabel zur Netzanbindung von Offshore-Windfarmen, Energiewirtschaft Vol. 4, No. 103, (in German).
9. BSH: Standard (2007). Konstruktive Ausführung von Offshore-Windenergieanlagen. Hambnurg und Rostock 2007. BSH-Nr. 7005 (in German).
10. Newson T A and Brunning P (2004). Thermal Conductivity of Deepwater Offshore Sediments, International Journal of Offshore and Polar Engineering, Vol. 14, No. 4, December 2004.
11. Wright J F et al. (2002). Thermal Conductivity of Sediments …., Geological Survey of Canada, Bulletin 585, 2002.
12. VDI Richtlinie 4640, Blatt 1 (2000). Thermische Nutzung des Untergrundes, Table 1. Beuth Verlag, Berlin, Germany.
13. Smolczyk U (2001). Grundbau Taschenbuch Teil 2, Geotechnische Verfahren: Anhaltswerte zur Wärmeleitfähigkeit wassergesättigter Böden, Ernst & Sohn-Verlag, Berlin.
14. Hillel D (1982). Introduction to Soil Physics, Academic Press, San Diego, CA, USA.
15. Cigré WG 21.02 (1997). Recommendations for Mechanical Tests on Sub-Marine Cables, Electra No. 171, April 1997.
16. Valenza D and Cipollini G (1995). HVDC Submarine Power Cable Systems – State of the Art and Future Developments, International Conference on Energy Management and Power Delivery, 1995. Proceedings of EMPD ′95.
17. Balog G et al. (1998). The Gulf of Aqaba Submarine Cable Link. Cigré paper 21-302, Cigré Session 1998.
18. Hauge O et al. (1988) Performance of the ± 250 kV HVDC Skagerrak Submarine Cables, IEEE Transactions Power Delivery, Vol. 3, No.1, January 1988.
19. Environmental Conditions and Environmental Loads, Recommended Practice DNV-RP-C205 issued by Det Norske Veritas, Norway, April 2007, Amended April 2008.

20. Balog G et al. (2006). Vortex Induced Vibration on Submarine Cables, Cigré Paper B1-208, Cigré Session 2006.
21. Vandiver J K et al. (1988). Predicted and Measured Response of flexible Cylinders in sheared Flow, Proceedings ASME Winter Annual Meeting, Symposium on Flow-Induced Vibration, Chicago, December 1988.
22. Kim Y H et al. (1985). Vortex-Induced Vibration and Drag Coefficients of Long Cables Subjected to Sheared Flows. Proceedings of Fourth International Offshore Mechanics and Arctic Engineering Symposium, ASME, Dallas, TX, February 17–21, 1985.
23. McAllister D (1982). Electric Cables Handbook, Granada Technical Books Ltd, 1982, ISBN 0-246-11467-3.
24. Bartnikas R (Ed.) (2000). Power and Communication Cables, IEEE Press Series on Power Engineering, ISBN 0-7803-1196-5.
25. Personal Communication Ulf Nilsson, Borealis, Sweden.
26. Bernard G (1989). Application of Weibull Distribution to the Study of Power Cable Insulation, Electra No.127, December 1989.
27. Chan J C et al. (1988). Comparative Performances of EPDM Versus XLPE as Insulation for Distribution Cables, RGE-No. 3-Mars 1988.
28. AEIC Cs9-06 (2006). Specifications for Extruded Insulation Power Cables and Their Accessories Rated above 46 KV through 345 KV (1st Edition). Association of Edison Illuminating Companies, USA.
29. Beyer M et al. (1986). Hochspannungstechnik, Springer, Berlin, Heidelberg, New York, London, Paris, Tokyo, 1986, ISBN 3-540-16014-0.
30. Worzyk T (2007). 100 Years of High Voltage DC Links, Modern Power Systems, Vol. 27, No. 11, pp. 21–24.
31. Boggs S et al. (2001). Effect of Insulation Properties on the Field Grading of Solid Dielectric DC Cable, IEEE Transactions on Power Delivery, Vol. 16, No. 4, pp. 456ff, October 2001.
32. Jeroense M J P (1997). Charges and Discharges in HVDC Cables: in Particular in Mass-Impregnated HVDC Cables, Ph.D. Thesis, Delft University of Technology, The Netherlands, 1997, also published as ISBN 90-407-1438-X, Delft University Press.
33. Bambery K et al. (1996). The Temperature Dependence of Space Charge Accumulation in Crosslinked Polyethylene, IEEE International Symposium Electrets, pp. 16–21.
34. Lim F N et al. (1999). The Temperature Dependence of Space Charge Accumulation and dc Current in XLPE Power Cable Insulation, IEEE Conference on Electrical Insulation Dielectric Phenomena (CEIDP), pp. 66–69.
35. Chong Y L et al. (2007). Temperature Effect on Space Charge Dynamics in XLPE Insulation, IEEE Transactions on Dielectrics and Electrical Insulation, Vol. 14, No. 1, pp. 65–76, February 2007.
36. Eoll C K (1975). Theory of Stress Distribution in Insulation of High-Voltage DC Cables: Part 1, IEEE Transaction on Electrical Insulation, Vol. Ei-10, No. 1, pp. 27–35, March 1975.
37. Schjölberg-Henriksen (1933). Transmission d'énergie électrique par courant continu à de très haute tensions. Berichte der Hochspannungskonferenz, Paris, 1933 (in French).